Spectroscopic and Electronic Structural Studies of the Cu(III)$_2$ Bis-μ-oxo Core and Its Relation to the Side-On Peroxo-Bridged Dimer

**Mark J. Henson, Pulakesh Mukherjee, David E. Root, T. D. P. Stack, and Edward I. Solomon***

Contribution from the Department of Chemistry, Stanford University, Stanford, California 94305

Received June 2, 1999

Abstract: Recently a Cu(III)$_2$ bis-μ-oxo dimer ligated by peralkylated amines has been found to interconvert with the side-on peroxo-bridged, μ-η^2:η^2 isomer. The Cu(III)$_2(\mu$-O)$_2$ dimer exhibits two intense charge transfer (CT) features in the near-UV region of the electronic absorption spectrum. Laser excitation into the lower-energy CT absorption band at 25 000 cm^{-1} results in intense resonance enhancement of the Raman peaks at 609 and 118 cm^{-1} which profile this band and give overtone and combination progressions. The combined application of a normal coordinate analysis of the Raman features and a time-dependent Heller theory analysis of the electronic absorption spectrum and resonance Raman profiles provide the excited-state geometry. As this transition corresponds to an oxo-to-Cu(III) CT, this excited state is formally an oxyl−Cu(II) species. Density functional calculations correlated to these data (including the excited-state geometry and the relative CT intensities) allow for an unambiguous assignment of the observed charge-transfer transitions. This assignment shows that one of the CT features involves the same orbital origin as a corresponding transition in the side-on peroxo dimer, while the new, low-energy band ($\sim$25 000 cm^{-1}) only observed for the bis-μ-oxo species corresponds to an oxo σ_u* to Cu(III) d$_{xy}$ CT transition which is present when the O−O bond is cleaved. This study provides electronic structural insight into the relationship between the bis-μ-oxo and side-on peroxo-bridged Cu species and their relative reactivities.

Introduction

The Cu(II)$_2$ side-on peroxo-bridged (μ-η^2:η^2) dimeric structural motif (Figure 1, left) is prominent in copper/O$_2$ bioinorganic chemistry. It was first characterized in a copper model complex synthesized by Kitajima and co-workers[1] and is present at the active sites of the O$_2$-binding protein oxyhemocyanin, the monooxygenase oxytyrosinase, and the catechol oxidases.[2] The side-on peroxo dimer has unique spectral features which are now well understood. The highest occupied peroxide orbitals are the degenerate π* levels. When peroxide binds to the metals these levels split in energy. The π_σ* (Op$_x$−Op$_x$: Figure 2, bottom) lies in the Cu$_2$O$_2$ plane and has direct σ-overlap with the half-occupied Cu(II) d$_{xy}$ orbitals,[3] while the π_v* (Op$_z$−Op$_z$: Figure 2, center) is perpendicular to this plane with a smaller π-bonding interaction with the Cu's. The electronic absorption spectrum of the side-on peroxo species shows intense charge transfer (CT) bands at 20 000 cm^{-1} (ϵ = 1000 M^{-1} cm^{-1}) and 28 000 cm^{-1} (ϵ = 20 000 M^{-1} cm^{-1}) which are assigned as the
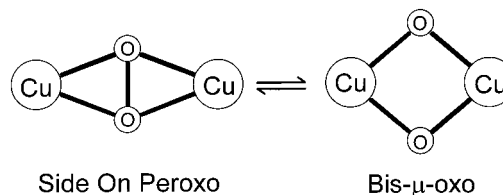
Figure 1. Cu$_2$O$_2$ core geometries of the side-on peroxo-bridged, μ-η^2:η^2 (left) and bis-μ-oxo (right) dimers.

O$_2^{2-}$ π_v* and π_σ* to Cu(II) d$_{xy}$ CT transitions, respectively.[4] In addition, resonance Raman (rR) studies show a low-energy ν(O−O) stretch at 740−750 cm^{-1}. This low stretching frequency reflects a weakened O−O bond which is due to a back-bonding interaction in the HOMO from the Cu d$_{xy}$ orbitals into the in-plane, high-energy unoccupied O$_2^{2-}$ σ_u* (σ-antibonding, Op$_y$+Op$_y$) orbital (Figure 2, top).

Side-on peroxo model dimers have recently been observed by Tolman and co-workers[5,6] to rearrange under certain conditions to form a bis-μ-oxo copper dimer (Figure 1, right). The bis-μ-oxo species has been obtained using both tridentate[7] and

(1) (a) Kitajima, N.; Fujisawa, K.; Moro-oka, Y.; Toriumi, K. *J. Am. Chem. Soc.* **1989,** *111,* 8975−8976. (b) Kitajima, N.; Fujisawa, K.; Moro-oka, Y.; Hashimoto, S.; Kitagawa, T.; Toriumi, K.; Tatsumi, K.; Nakamura, A. *J. Am. Chem. Soc.* **1992,** *114,* 1277−1291.

(2) (a) Solomon, E. I.; Sundaram, U. M.; Machonkin, T. E. *Chem. Rev.* **1996,** *96,* 2563−2605. (b) Magnus, K. A.; Ton-That, H.; Carpenter, J. E. *Chem. Rev.* **1994,** *94,* 727−735. (c) Rompel, A.; Fischer, H.; Büldt-Karentzopoulos, K.; Meiwes, D.; Zippel, F.; Nolting, H.- F.; Hermes, C.; Krebs, B.; Witzel, H. *J. Inorg. Biochem.* **1995,** *59,* 715.

(3) A dimeric coordinate frame is used, with the Cu−Cu vector lying along the *x*-axis and the O−O vector along the *y*-axis. This coordinate system has the lobes of the Cu d$_{xy}$ orbitals oriented along the M−L bonds. This differs from monomeric coordinate systems have the d$_{x^2-y^2}$ lobes oriented along the M−L bonds.

(4) (a) Ross, P. K.; Solomon, E. I. *J. Am. Chem. Soc.* **1991,** *113,* 3246−3259. (b) Solomon, E. I.; Tuczek, F.; Root, D. E.; Brown, C. A. *Chem. Rev.* **1994,** *94,* 827−856.

(5) (a) Halfen, J. A.; Mahapatra, S.; Wilkinson, E. C.; Kaderli, S.; Young, V. G., Jr.; Que, L., Jr.; Zuberbühler, A. D.; Tolman, W. B. *Science* **1996,** *271,* 1397−1400.

(6) (a) Mahapatra, S.; Kaderli, S.; Llobet, A.; Neuhold, Y.-M.; Palanché, T.; Halfen, J. A.; Young, V. G., Jr.; Kalden, T. A.; Que, L., Jr.; Zuberbühler, A. D.; Tolman, W. B. *Inorg. Chem.* **1997,** *36,* 6343−6356. (b) Mahapatra, S.; Halfen, J. A.; Tolman, W. B. *J. Am. Chem. Soc.* **1996,** *118,* 11575−11586.

Studies of the Cu(III)$_2$ Bis-μ-oxo Core

J. Am. Chem. Soc., Vol. 121, No. 44, 1999 10333
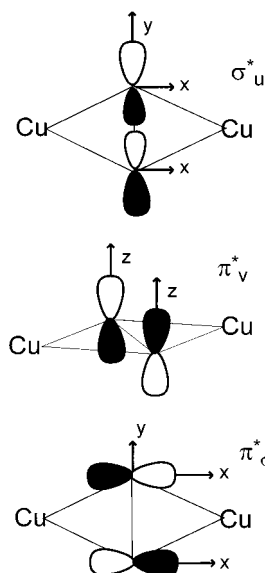
Figure 2. The peroxo orbitals which serve as donors for the charge-transfer transitions observed for the side-on peroxo dimer are the out-of-plane π_v^* (middle) and the in-plane π_σ^* (bottom). The high energy, in-plane unoccupied σ_u^* (top) has a bonding interaction with the Cu (II) d$_{xy}$ orbitals in the side-on peroxo dimer. This leads to π-back-bonding into the σ_u^* which weakens the O–O bond.

bidentate[8] amine ligand systems, both of which give Cu$_2$O$_2$ cores with short Cu–O bond lengths of 1.80 Å and Cu$\cdots$Cu and O$\cdots$O separations of 2.73–2.88 (by EXAFS) and 2.28–2.34 Å, respectively. XAS studies have shown this complex to involve two Cu(III)'s.[9] Thus the O atoms are reduced to the oxide level, and the long O$\cdots$O separation indicates that there is no longer an O–O bond. The side-on peroxo and bis-μ-oxo structural isomers have been found to be in a rapid equilibrium, attributed to a flat potential surface for interconversion.[10] As this involves reversible O–O bond cleavage, it is an electronic process with significant chemical/mechanistic implications.

The Cu(III)$_2$ bis-μ-oxo dimer also has unique spectral features: an intense CT absorption band at approximately 22 000–26 000 cm^{-1} (ϵ = 13 000–28 000 M^{-1} cm^{-1}) and a similarly intense band at 31,000–34 000 cm^{-1} (ϵ = 11 000–21 000 M^{-1} cm^{-1}).[7,8,11] These features can provide direct experimental insight into the electronic structure of the Cu(III)$_2$ bis-μ-oxo core. The high energies and intensities of the bands (relative to d → d transitions) are consistent with charge-transfer transitions arising from a high degree of Cu/O covalency within this species.

The purpose of this study is to evaluate these spectral features to describe the electronic structure and bonding in the Cu(III)$_2$ bis-μ-oxo dimers. As in our past studies of binuclear Cu oxygen species,[4,12–14] this investigation combines electronic absorption

spectroscopy, vibrational analysis, resonance Raman profiles, and electronic structural calculations. Further, the nature of the resonance Raman overtone and profile data obtained for the bis-μ-oxo complex (*vide infra*) allows this analysis to be extended to the quantitation of the excited-state distortion corresponding to the 25 000 cm^{-1} CT transition, which provides valuable information about the bonding within both the electronic ground state and the lowest-energy CT excited state of this species. Since this transition involves transfer of e$^-$ density from the oxo ligand to the Cu(III), this CT excitation results in a species which can be formally described as an oxyl–Cu(II) complex. The spectroscopic description that is obtained for the bis-μ-oxo species is correlated to the side-on peroxo dimer to obtain insight into the mechanism of O–O bond cleavage, factors that influence the interconversion between these structural isomers, and the differences in their reported reactivity. In particular, the origin of the increase in H-atom abstraction reactivity for the bis-μ-oxo structure relative to the side-on peroxo will be addressed.[6]

Experimental Methods

Sample Preparation. All bis-μ-oxo samples were prepared as described previously.[8] The ligands employed in this study were alkyl-substituted cyclohexyldiamines, tetraethylethylenediamine (L^{TEED}), and tetramethylpropylenediamine (L^{TMPD}). Primary focus is on the structurally defined bis-μ-oxo dimer using the *N,N*′-dimethyl-*N,N*′-diethylcyclohexyldiamine (L^{MECHD}) ligand.[8]

Resonance Raman. Resonance Raman (rR) spectra were obtained using a Princeton Instruments ST-135 back-illuminated CCD detector on a Spex 1877 CP triple monochromator with 1200, 1800, and 2400 grooves/mm holographic spectrograph gratings. Excitation was provided by Coherent I90C-K Kr$^+$ and Innova Sabre 25/7 Ar$^+$ CW ion lasers. A polarization scrambler was used between the sample and the spectrometer. Spectral resolution was < 2 cm^{-1}.

The samples were prepared by dissolving the Cu(I) amine precursor in CH$_2$Cl$_2$ in 5 mm NMR tubes and oxygenating at 193 K. Typical rR solution sample concentrations were in the range of 5mM of Cu (2.5 mM of dimer) to minimize self-absorption. The samples were spun with an air-driven NMR spinner and cooled to ∼190 K by a N$_2$-flow system. Isotopic substitution was achieved by oxygenation with ^{18}O$_2$ (Isotech, 99% labeled).

Integrated peak intensities used to determine rR profiles were measured relative to the 700 cm^{-1} peak of CH$_2$Cl$_2$ for solution samples. The bis-μ-oxo ν = 609 cm^{-1} to CH$_2$Cl$_2$ 700 cm^{-1} integrated peak intensity ratio at λ_{ex} = 457.9 nm was arbitrarily set equal to 1.00 to scale the profile points. Variance in the CH$_2$Cl$_2$ 286 to 700 cm^{-1} ratio versus excitation frequency was used to compensate for self-absorption in the samples.

Resonance Raman profiles were simulated by using the time-dependent theory developed by Heller and co-workers[15a,b] within a Mathcad 7 script written by Dr. Thomas Brunold.[16]

Normal Coordinate Analysis. A normal coordinate analysis (NCA) was performed on the idealized D_{2h}-symmetric Cu$_2$O$_2$ core of the bis-μ-oxo dimer: Cu–O = 1.80 Å; O$\cdots$O = 2.34 Å. The analysis was

(7) Mahapatra, S.; Halfen, J. A.; Wilkinson, E. C.; Pan, G.; Wang, X.; Young, V. G., Jr.; Cramer, C. J.; Que, L., Jr.; Tolman, W. B. *J. Am. Chem. Soc.* **1996**, *118*, 11555−11574.

(8) Mahadevan, V.; Hou, Z.; Cole, A. P.; Root, D. E.; Lal, T. K.; Solomon, E. I.; Stack, T. D. P. *J. Am. Chem. Soc.* **1997**, *119*, 11996−11997.

(9) DuBois, J. L.; Mukherjee, P.; Collier, A. M.; Mayer, J. M.; Solomon, E. I.; Hedman, B.; Stack, T. D. P.; Hodgson, K. O. *J. Am. Chem. Soc.* **1997**, *119*, 8578−8579.

(10) (a) Cramer, C. J.; Smith, B. A.; Tolman, W. B. *J. Am. Chem. Soc.* **1996**, *118*, 11283−11287. (b) Bérces, A. *Inorg. Chem.* **1997**, *36*, 4831−4837. (c) Flock, M.; Pierloot, K. *J. Phys. Chem. A* **1999**, *103*, 95−102.

(11) Mahadevan, V.; DuBois, J. L.; Hedman, B.; Hodgson, K. O.; Stack, T. D. P. *J. Am. Chem. Soc.* **1999**, *121*, 5583−5584.

(12) Pidcock, E.; Obias, H. V.; Zhang, C. X.; Karlin, K. D.; Solomon, E. I. *J. Am. Chem. Soc.* **1998**, *120*, 7841−7847.

(13) Pidcock, E.; Obias, H. V.; Abe, M.; Liang, H.-C.; Karlin, K. D.; Solomon, E. I. *J. Am. Chem. Soc.* **1999**, *121*, 1299−1308.

(14) Pidcock, E.; DeBeer, S.; Obias, H. V.; Hedman, B.; Hodgson, K. O.; Karlin, K. D.; Solomon, E. I. *J. Am. Chem. Soc.* **1999**, *121*, 1870−1878.

(15) (a) Lee, S. Y.; Heller, E. J. *J. Chem. Phys.* **1979**, *71*, 4777. (b) Tannor, D. J.; Heller, E. J. *J. Chem. Phys.* **1982**, *77*, 202. (c) Myers, A. B.; Mathies, R. A. In *Biological Applications of Raman Spectroscopy*; Spiro, T. G., Ed.; Wiley: New York, 1987; Vol. 2, pp 1−58. (d) Zink, J. I.; Shin, K. S. K. *Adv. Photochem.* **1991**, *16*, 119.

(16) (a) Brunold, T. C.; Tamura, N.; Kitajima, N.; Moro-oka, Y.; Solomon, E. I. *J. Am. Chem. Soc.* **1998**, *120*, 5674−5690. (b) Brunold, T. C.; Gamelin, D. R.; Stemmler, T. L.; Mandal, S. K.; Armstrong, W. H.; Penner-Hahn, J. E.; Solomon, E. I. *J. Am. Chem. Soc.* **1998**, *120*, 8724−8738.
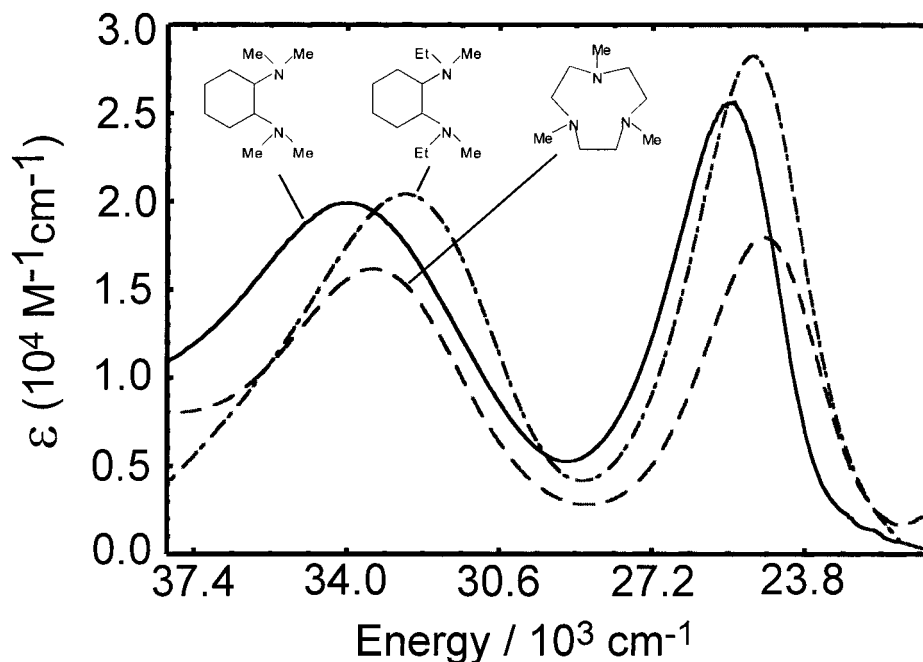
Figure 3. Bis-μ-oxo dimer solution electronic absorption spectra for three different ligand systems: L^{TMCHD} (—), L^{MECHD} (-•-•-•), and L^{ME_3TACN} (- - -) [all in dichloromethane at 193 K].

based on a Wilson FG matrix method using a Urey–Bradley force field as implemented in a modified version of the Schachtschneider program.[17]

Electronic Structure Calculations. All calculations were performed on simplified models in which the complex, substituted alkylamine ligands were replaced with NH$_3$ ligands. LCAO density functional calculations were performed using the 2.0.1 version of the Amsterdam Density Functional (ADF) programs.[18] The Vosko–Wilk–Nusair local density approximation (VWN LDA)[19] for the exchange and correlation energy was used with the nonlocal gradient corrections of Becke and Perdew[20,21] (included in the SCF process, though switching to a post-SCF correction resulted in minimal changes to both the total energy and the final wave function). A triple-ζ Slater-type orbital (STO) basis set with a single-ζ STO polarization function was used for all atoms. Filled shell orbitals were treated by the frozen core approximation. ADF 2.0.1 was used only to estimate total energies, as we have observed that the LDA method typically overestimates the covalency of Cu compounds relative to experimental data.

Electronic structure calculations using the 1982 QCPE version of the self-consistent field Xα scattered wave (SCF Xα-SW) package[22-27] were run on an IBM 397 and 3BT-RS/6000 computers. The exchange values, α, used in the atomic spheres are those of Schwarz[28] except in the case of H, for which an α of 0.777 25 was used.[29] The inter- and outer-sphere α values were the valence-electron weighted average of the atomic α values. Norman sphere radii were used for all atoms except copper.

In previous calculations on various Cu(II) complexes, a copper sphere radius of 2.95 bohr was used rather than the Norman radius of $\sim$2.3 bohr as it better reproduces the ground-state g values in CuCl$_4^{2-}$ and plastocyanin.[30,31] A problem arises with using such a large sphere radius in calculations on Cu(III)-containing complexes because of the much shorter Cu–ligand bonds. In the L^{MECHD} bis-μ-oxo dimer the average Cu–O bond length is 1.80 Å vs 1.92 Å in the μ-η^2:η^2 side-on peroxo complex.[1b] This gives a Cu/O sphere radius overlap of 41% in the bis-μ-oxo dimer vs 32% in the side-on peroxo dimer. Case et al.[32] noted that an interatomic sphere overlap of 40% or more gave erroneous answers. In our calculations involving Cu(III), a sphere radius range of 2.65–2.75 bohr was selected to give a Cu/O sphere radius overlap of 32–35%, which best fits experimental results and allows easy correlation to earlier calculations on the side-on peroxo isomer. Most computational results are reported for a Cu sphere radius of 2.75 bohr (35% overlap) except when significant differences arise between calculations using this range of sphere radii.

A Watson sphere with a radius equal to that of the outer sphere and charge equal but opposite to that of the model was included for ionic models unless otherwise noted. A relative change in the atomic potentials of less than 1×10^{-5} Rydbergs between iterations was used as a criterion for convergence. The coordinates of the models used for the SCF Xα-SW calculations are given in the Supporting Information (Table SM1). Charge-transfer energies were calculated using the Slater transition-state method.[23]

Results and Analysis

A. Absorption. The absorption spectra for a series of Cu bis-μ-oxo dimers show two intense absorption features at $\sim$22 000–26 000 (E_1) and $\sim$31 000–34 000 cm^{-1} (E_2) in the violet/near-UV region (Figure 3), as summarized in Table 1.

(17) (a) Schachtschneider, J. H. Technical Report No. 57-65; Shell Development Company: Emeryville, CA, 1966. (b) Fuhrer, H.; Kartha, V. B.; Kidd, K. G.; Krueger, P. J.; Mantsch, H. H. *Computer Programs for Infrared Spectroscopy*; Bulletin No. 15; National Research Council of Canada: Ottawa, 1976.

(18) te Velde, G.; Baerends, E. J. *J. Comput. Phys.* **1992**, *99*, 84–98.

(19) Vosko, S. H.; Wilk, L.; Nusair, M. *Can. J. Phys.* **1980**, *58*, 1200–1211.

(20) Becke, A. D. *Phys. Rev. Rev. A* **1988**, *38*, 3098–3100.

(21) Perdew, J. P. *Phys. Rev. B* **1986**, *33*, 8800–8802.

(22) Cook, M.; Case, D. A. *QCPE Program 465* **1991**, *23*, 21–22.

(23) Slater, J. C. *The Self-Consistent Field for Molecules and Solids: Quantum Theory of Molecules and Solids*; McGraw-Hill: New York, 1974; Vol. 4.

(24) Johnson, K. H.; Norman, J. G., Jr.; Connolly, J. W. D. *Computational Methods for Large Molecules and Localized States in Solids*; Plenum: New York, 1973.

(25) Connolly, J. W. D. *Semiempirical Methods of Electronic Structure Calculation, Part A: Techniques*; Plenum: New York, 1977.

(26) Cook, M. R., Ph.D. Thesis, Havard University, 1981.

(27) Case, D. A. *Annu. Rev. Phys. Chem.* **1982**, *33*, 151–171.

(28) Schwartz, K. *Phys. Rev. B* **1972**, *5*, 2466–2468.

(29) Slater, J. C. *Int. J. Quantum Chem., Quantum Chem. Symp.* **1973**, *7*, 533–544.

(30) Gewirth, A. A.; Cohen, S. L.; Schugar, H. J.; Solomon, E. I. *Inorg. Chem.* **1987**, *26*, 1133–1146.

(31) Gewirth, A. A.; Solomon, E. I. *J. Am. Chem. Soc.* **1988**, *110*, 3811–3819.

(32) Case, D. A.; Huynh, B. H.; and Karplus, M. *J. Am. Chem. Soc.* **1979**, *101*, 4433–4453.

Table 1[a]

complex	E_1/cm^{-1} ($\epsilon/M^{-1}\,cm^{-1}$)	E_2/cm^{-1} ($\epsilon/M^{-1}\,cm^{-1}$)	EXAF Cu···Cu/Å	X-ray Cu···Cu/Å	ref
(CN = 4) Systems					
$[(L^{TMCHD}Cu)_2(\mu\text{-}O)_2]^{2+}$	25 500 (25 000)	34 000 (20 000)			8
$[(L^{MECHD}Cu)_2(\mu\text{-}O)_2]^{2+}$	25 000 (28 000)	32 700 (21 000)	2.73	2.743	8,9
$[(L^{TECHD}Cu)_2(\mu\text{-}O)_2]^{2+}$	24 600 (23 000)	32 000 (17 000)			8
$[(L^{TEED}Cu)_2(\mu\text{-}O)_2]^{2+}$	25 000 (24 000)	33 300 (17 000)	2.75		9
(CN = 5) Systems					
$[(L^{Me_3TACN}Cu)_2(\mu\text{-}O)_2]^{2+}$	24 700 (18 000)	33 300 (16 000)	2.77		11
$[(L^{iPr_4dtne})Cu_2(\mu\text{-}O)_2]^{2+}$	24 200 (14 000)	31 600 (13 000)		2.783	33
$[(L^{Bn_3TACN}Cu)_2(\mu\text{-}O)_2]^{2+}$	23 300 (14 000)	31 400 (12 000)	2.84–2.86[b]	2.794	7
$[(L^{iPr_2BnTACN}Cu)_2(\mu\text{-}O)_2]^{2+}$	22 900 (16 000)	31 100 (12 000)			7
$[(L^{iPr_3TACN}Cu)_2(\mu\text{-}O)_2]^{2+}$	22 300 (13 000)	30 900 (11 000)	2.88[b]		7

[a] L^{TMCHD} = *N,N,N′,N′*-tetramethylcyclohexyldiamine. L^{MECHD} = *N,N′*-dimethyl-*N,N′*-diethylcyclohexyldiamine. L^{TECHD} = *N,N,N′,N′*-tetraethylcyclohexyldiamine. L^{TEED} = *N,N,N′,N′*-tetraethylethylenediamine. L^{Me_3TACN} = 1,4,7-trimethyl-1,4,7-triazocyclononane. L^{iPr_4dtne} = 1,2-bis(4,7-diisopropyl-1,4,7-triaza-1-cyclononyl)ethane. L^{Bn_3TACN} = 1,4,7-tribenzyl-1,4,7-triazocyclononane. $L^{iPr_2BnTACN}$ = 1,4-diisopropyl-7-benzyl-1,4,7-triazocyclononane. L^{iPr_3TACN} = 1,4,7-triisopropyl-1,4,7-triazocyclononane. [b] Note: As described in ref 7, the discrepancy between EXAFS and X-ray Cu···Cu distances may be due to limited resolution of the second shell scattering associated with both Cu and ligand backbone carbons.

The high intensity of these features are consistent with charge-transfer transitions, presumably oxo to Cu(III) given the established electronic structural description of these dimers from Cu K-edge studies.[9] These transitions are relatively low in energy for ligand-to-metal charge transfer (LMCT) bands. This fact, along with the high intensities, is indicative of a high degree of Cu–O covalency.

An interesting trend in CT transition energies exists over the range of dimers listed in Table 1. This trend correlates with two major structural changes, closely coupled, that arise from variation of the amine ligand system employed in dimer formation (Note that only ligands which contain 2-carbon bridges between nitrogens are considered in this analysis). First, the CT energies could be affected by a change in Cu coordination number from four to five ligands (square planar to square pyramidal). Tridentate (triazocyclononane, TACN) ligands result in formation of bis-μ-oxo dimers that have 5-coordinate Cu atoms,[7,11] while the cyclohexyldiamine (CHD) ligands used here give 4-coordinate Cu atoms. The absorption spectra of the dimers with 5-coordinate Cu ligation mostly exhibit a decrease in CT transition energies (~3000 cm⁻¹ lower in energy than the E_1 and E_2 CT features observed for the CHD-based dimers).

Further, these changes in CT transition energies are closely linked to changes in the Cu_2O_2 core geometry. This is clearly reflected in the large variance in Cu···Cu distance with changes in number of ligands on the metal as well as increases in the steric bulk of the ligand N-alkyl substituents. From EXAFS and X-ray crystallographic results[7–9,11,33] longer Cu···Cu separations are observed in the dimers formed with the TACN (≥2.77 Å) ligands relative to the bidentate CHDs (2.73–2.75 Å). Longer intermetal distances correlate with the lower-energy CT transitions [L^{MECHD} has $r_{Cu···Cu}$ = 2.74 Å (X-ray) with E_1 = 25 000 cm⁻¹ and E_2 = 32 700 cm⁻¹, while L^{Bn_3TACN} has $r_{Cu···Cu}$ = 2.79 Å (X-ray) with E_1 = 23 300 cm⁻¹ and E_2 = 31 400 cm⁻¹]. In addition, there are minor energetic trends within the subsets of ligands with the same coordination number that seem to be linked to the donor properties and/or steric bulk of the N-alkyl substituents. For instance, within the set of tridentate TACN-based ligands, E_1 and E_2 decrease by 1400 and 1900 cm⁻¹ (and the Cu···Cu distance increases from 2.77 to 2.79 Å), respectively, as the ligand N-alkyl substituents are varied from methyl to benzyl groups. The relative contributions of the metal to metal distance and coordination number to the CT transition energies will be evaluated in Section E.

B. Resonance Raman. A sharp feature in the 600–700 cm⁻¹ region of the Raman spectrum has proven to be diagnostic of the bis-μ-oxo dimer core vibration for a number of metals: Cu (600–616 cm⁻¹),[7,8,11] Fe,[34,35] and Mn.[36] Similarly, the Raman spectrum for the L^{MECHD} dimer is characterized by an intense feature at 609 cm⁻¹ (Figure 4). Three features (491, 609, and 727 cm⁻¹) show a $\Delta\nu$ = –23 to –24 cm⁻¹ shift upon $^{18}O_2$ substitution (Figure 4). These three isotope-sensitive peaks are each separated by 118 cm⁻¹. An isotope-insensitive 118 cm⁻¹ fundamental exists and is of significant intensity for such a low-frequency feature. This, combined with the uniform isotope shift of all 3 bands, indicates that the ν = 491 and 727 cm⁻¹ features are in fact difference ($\nu_{491} = \nu_{609} - \nu_{118}$) and combination ($\nu_{727} = \nu_{609} + \nu_{118}$) bands formed from the ν = 118 and 609 cm⁻¹ fundamentals. In addition, the relative intensity of the 491 cm⁻¹ band decreases as the sample temperature is lowered from 193 to 77 K, confirming the difference band assignment. This feature reflects an anti-Stokes hot band transition of the 118 cm⁻¹ mode whose intensity is proportional to the Boltzmann thermal population of an excited vibrational state. Since resonance Raman (rR) intensity is proportional to the squares of the modal frequency and the dimensionless excited-state distortion parameter Δ, the relatively high intensity of the feature at 118 cm⁻¹ indicates that it plays an important role in determining the CT excited-state geometry of the bis-μ-oxo dimer. This will be addressed in Section D.

The ν_1 (= 118 cm⁻¹) and ν_3 (= 609 cm⁻¹) vibrations show only slight frequency shifts when different diamine ligand systems are employed (Table 2).[8] For example, ν_3 shifts to 605 (–4 cm⁻¹) in the L^{TMCHD} dimer and 616 (+7 cm⁻¹) in the L^{TECHD} dimer. The ν_1 band does not shift beyond experimental error upon changing the CHD N-alkyl substituent(s), but shifts to 133 cm⁻¹ in the L^{TMPD} dimer. The relatively small changes in these modal frequencies, as well as the magnitude of the $^{18}O_2$ shift for ν_3, indicate that these modes may be well represented using only the four atoms of the Cu_2O_2 core, which will be used in the normal coordinate analysis (*vide infra*). Several O_2 isotope-independent peaks exist in the rR spectra which show

(33) Mahapatra, S.; Young, V. G., Jr.; Kaderli, S.; Zuberbühler, A.; Tolman, W. B. *Angew. Chem., Int. Ed. Engl.* **1997**, *36*, 130–133.

(34) Dong, Y.; Fujii, H.; Hendrich, M. P.; Leising, R. A.; Pan, G.; Randall, C. R.; Wilkinson, E. C.; Zang, Y.; Que, L., Jr.; Fox, B. G.; Kauffmann, K.; Münck, E. *J. Am. Chem. Soc.* **1995**, *117*, 2778–2792.

(35) Wilkinson, E. C.; Dong, Y.; Zang, Y.; Fujii, H.; Fraczkiewicz, R.; Fraczkiewicz, G.; Czernuszewicz, R. S.; Que, L., Jr. *J. Am. Chem. Soc.* **1998**, *120*, 955–962.

(36) Czernuszewicz, R. S.; Dave, B.; Rankin, J. G. In *Spectroscopy of Biological Molecules*; Hester, R. E., Girling, R. B., Eds.; Royal Society of Chemistry: Cambridge, 1991; pp 285–288.
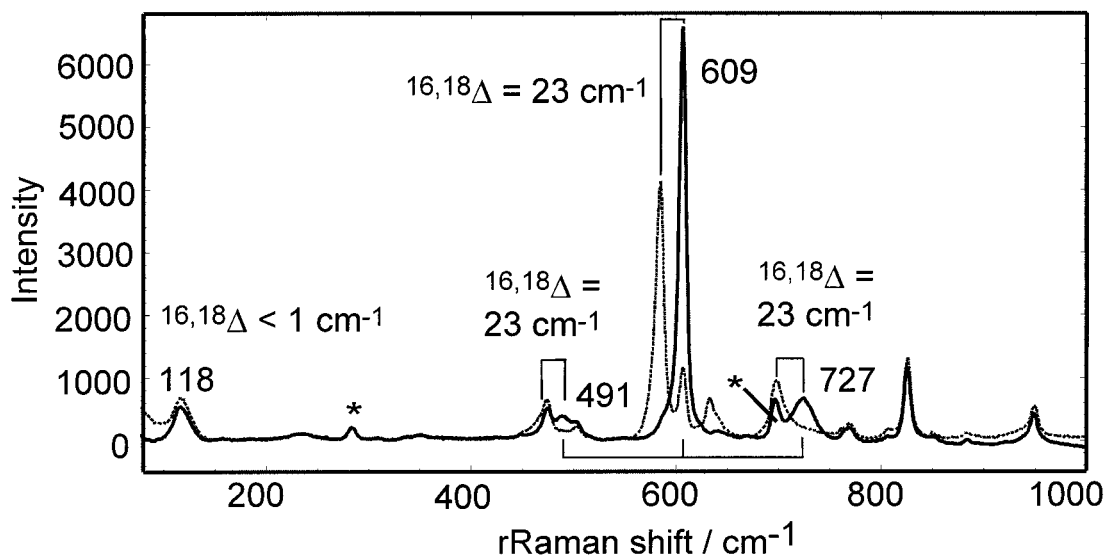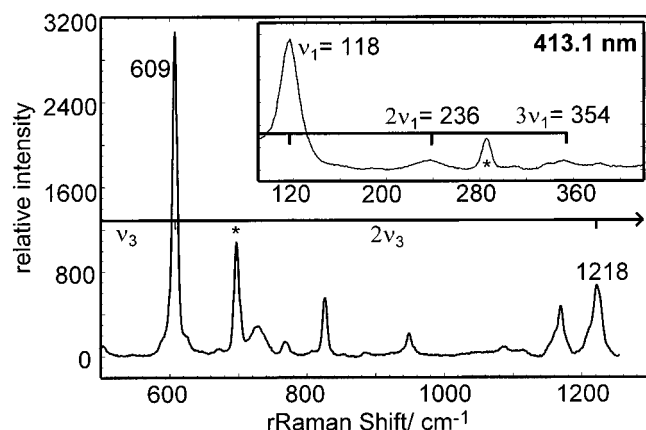
Figure 4. Resonance Raman spectrum of $^{16}O_2$ (——) and $^{18}O_2$ (- - -) substituted 5mM $[(L^{MECHD}Cu)_2(\mu\text{-}O)_2]^{2+}$ in dichloromethane at 193 K (λ_{ex} = 406.7 nm). Solvent peaks at 286 and 700 cm^{-1} are indicated by asterisks (*).

Table 2

ligand	ν_1	ν_2	ν_3 ($^{16}O_2/^{18}O_2$ shift)	ν_4	ν_5
TMPD	133	509 (s)	608 ($\Delta = -27$)		956 (w)
TEPD	133	517 (s)	613 ($\Delta = -28$)		962 (w)
TMCHD	118	501 ± 1 (w)	605 ($\Delta = -23$)	841 (m)	a
MECHD	118	476, 504 (w)	609 ($\Delta = -23$)	827 (m)	951 (w)
TECHD	118	a	616 ($\Delta = -26$)	a	a

^{a} Spectral noise did not allow detection of peaks.

Figure 5. Resonance Raman spectrum of $[(L^{MECHD}Cu)_2(\mu\text{-}O)_2]^{2+}$ in dichloromethane at λ_{ex} = 413.1 nm, showing overtone peaks at $2\nu_1$ = 236 cm^{-1}, $3\nu_1$ = 354 cm^{-1} (inset), and $2\nu_3$ = 1218 cm^{-1}.

larger shifts with small perturbations in the diamine ligand, and major frequency and intensity changes with significant perturbations. The $^{18}O/^{16}O$-insensitive vibrations in the 470−520 cm^{-1} region (Figure 4) that are variable among the ligands (e.g., ν_2 in Table 2) can thus be assigned as Cu−N stretching modes, which would be highly ligand-dependent.

At peak resonance (λ_{ex} = 413.1 nm), the Raman spectra clearly display overtone progressions (Figure 5) along the ν_1 and ν_3 modes. Members of a progression in ν_1 appear at approximately $2\nu_1$ = 236 and $3\nu_1$ = 354 cm^{-1}, both with $\Delta\nu(^{16,18}O_2)$ = 0, for L^{MECHD}. A similar progression is observed for L^{TMPD} (ν_1 = 133 cm^{-1}): 266 and 400 cm^{-1}, both also with $\Delta\nu^{16,18}$ = 0. These peaks also correspond to $2(\nu_1)$ and $3(\nu_1)$, respectively. There is also a progression of bands at 1218 ($\Delta\nu^{16,18} = -46 \pm 1$) and 1827 ($\Delta\nu^{16,18} = -70$) for L^{MECHD} which correspond to $2(\nu_3)$ and $3(\nu_3)$. As mentioned above, the

ν_1 and ν_3 fundamentals combine to form sum and difference bands. The ν_1 fundamental is also observed to form a combination with the first overtone of ν_3 at 1336 cm^{-1} ($\nu_1 + 2\nu_3$ = 118 + 1218; $\Delta = -45 \pm 1$ cm^{-1}) as illustrated in Figure S1, Supporting Information. The formation of combination bands indicates that the excited state undergoes a geometric distortion simultaneously along both of these modes. Their intensities and the observation of overtone progressions indicates that the distortions along ν_1 and ν_3 are large.

The amine ligand-type vibrational modes also form combination bands with ν_3. For example, combinations are observed at 1085 (609 + 476), 1436 (609 + 827), and 1559 cm^{-1} (609 + 950) for L^{MECHD}. Each of these bands are observed to shift by -23 cm^{-1} upon $^{18}O_2$ substitution, consistent with their assignments as combinations of ν_3 with 3 different isotope-insensitive modes (Figure S1). As for ν_1 and ν_3, the observation of the combinations ($\nu_3+\nu_2$), ($\nu_3+\nu_4$), and ($\nu_3+\nu_5$) has implications for the excited-state geometric distortion along the ν_2, ν_4, and ν_5 modes (*vide infra*).

The ν_1 and ν_3 modes (and their combination at 728 cm^{-1}) show intense resonance enhancement which profiles the 25 000 cm^{-1} charge-transfer band (Figure 6). Preresonance enhancement for the 32 700 cm^{-1} CT is also observed, but this band is too high in energy for us to probe. The amine ligand-type bands also show resonance enhancement, to a lesser degree, which follows the 25 000 cm^{-1} CT band. This fact, along with their combination bands with the ν_3 fundamental, indicates that the excited-state distortion is also delocalized over the amine ligand vibrational modes, not an unreasonable result considering the nature of the resonant electronic transition. A large Cu−N bond length change would be anticipated for an $O^{2-} \rightarrow$ Cu(III) LMCT. From EXAFS data, the average Cu(III)-N bond length for the L^{TEED} bis-μ-oxo dimer is 1.93 Å,[9] which lengthens to 2.00 Å upon reduction in the Cu(II) bis-hydroxo dimer. Thus a significant excited-state distortion is anticipated to occur along the Cu/amine mode(s) upon charge transfer. The delocalization of the distortion beyond the four atoms of the Cu$_2$O$_2$ core is also consistent with a highly covalent electronic structural description of the bis-μ-oxo dimer.

However, these ligand-type modes can be justifiably disregarded in a quantitation of the excited-state distortion of the Cu$_2$O$_2$ core for a number of reasons. First, ligand variation only
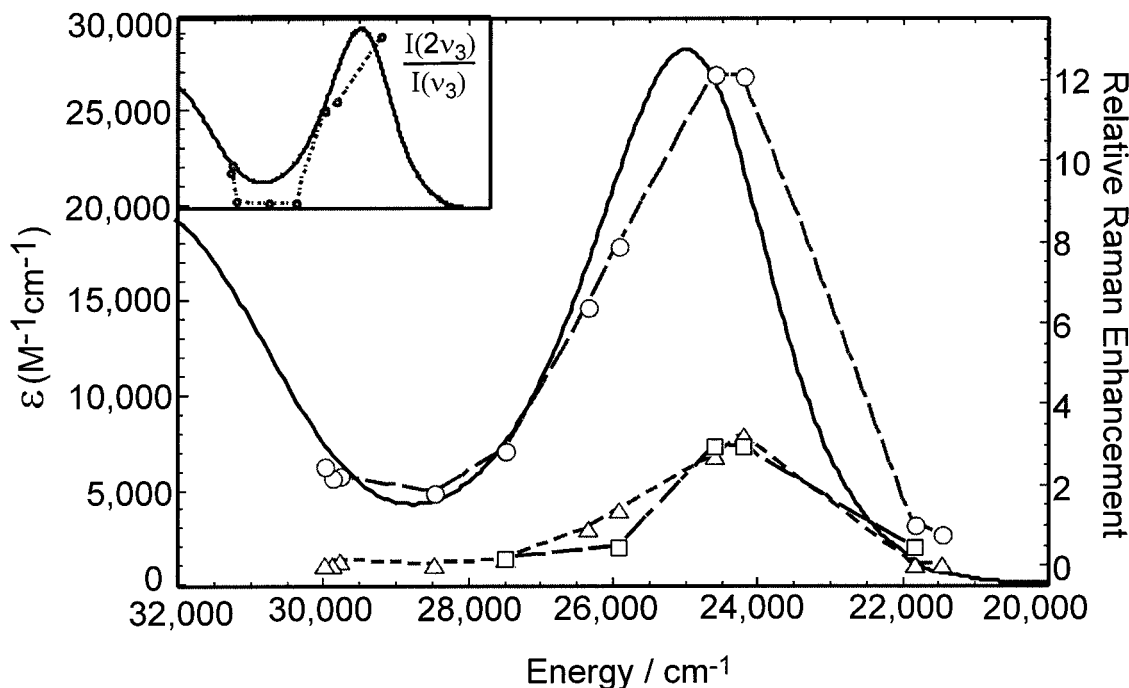
Figure 6. Electronic absorption spectrum of $[(L^{MECHD}Cu)_2(\mu\text{-}O)_2]^{2+}$ (—) with superimposed resonance Raman profiles for the peaks at $\nu_1 = 118$ cm^{-1} (□), $\nu_3 = 609$ cm^{-1} (○), and $(\nu_1+\nu_3) = 727$ cm^{-1} (△). Inset is the plot of the $2\nu_3/\nu_3$ overtone-to-fundamental ratio vs excitation wavelength.

Table 3

normal mode	$\delta_s(\text{O}-\text{Cu}-\text{O})$ a$_g$	$\delta_{as}(\text{Cu}-\text{O}-\text{Cu})$ b$_{2u}$	$\nu_s(\text{Cu}-\text{O})$ a$_g$	$\nu_{as}(\text{Cu}-\text{O})$ b$_{1g}$	$\delta_{as}(\text{O}-\text{Cu}-\text{O})$ b$_{3u}$
obsd $^{16}O_2/^{18}O_2$ (shift)	118/118 (0)		609/586 (−23)		
NCA $^{16}O_2/^{18}O_2$ (shift)	118.6/117.2 (−1.4)	549.9/524.9 (−25.0)	611.5/583.4 (−28.1)	625.9/595.8 (−30.1)	643.7/614.4 (−29.3)
k (mdyne/Å)	0.297^a		2.699^b		
L_1 (Cu−O)$_1$ (PED)	0.01023 (13.6)	−0.12847 (100)	0.13277 (86.4)	−0.14624 (100)	−0.15038 (100)
L_2 (Cu−O)$_2$	0.01023	0.12847	0.13277	0.14624	−0.15038
L_3 (Cu−O)$_3$	0.01023	−0.12847	0.13277	0.14624	0.15038
L_4 (Cu−O)$_4$	0.01023	0.12847	0.13277	−0.14624	0.15038
L_5 (O−O) (PED)	−0.15514 (86.4)	0.00000 (0.0)	0.31770 (13.6)	0.00000 (0.0)	0.00000 (0.0)

$^a = k_{\text{O}-\text{O}}$ (not modal force constant). $^b = k_{\text{Cu}-\text{O}}$.

slightly perturbs the frequencies and resonance intensities of the ν_1 and ν_3 modes. Second, more limited enhancements are observed along these modes relative to ν_1 and ν_3. Last, these modes are insensitive to $^{18}O_2$ substitution, indicating a lack of Cu−O motion mixed into these modes.

C. Normal Coordinate Analysis. Based on these Raman data, a normal coordinate analysis (NCA) was performed on the 4-atom D_{2h} Cu$_2$O$_2$ core of the bis-μ-oxo dimer. Five internal coordinates were used: the 4 Cu−O stretches ($r_{\text{Cu}-\text{O}} = 1.80$ Å) and a nonbonded O···O interaction ($r_{\text{O}\cdots\text{O}} = 2.34$ Å). An initial estimate of $k_{\text{Cu}-\text{O}} = 3.00$ mdyne/Å was based upon previous Fe oxo dimer studies,[35] and the low initial estimate of $k_{\text{O}-\text{O}} = 0.300$ mdyne/Å was based upon large the O···O separation. Out of plane motion was not considered in the analysis, which is justified by the excellent correspondence of the experimental and calculated frequencies and isotope shifts. Inputing only the experimental $\nu_3(^{16}O_2) = 609$ cm^{-1} and $\nu_3(^{18}O_2) = 586$ cm^{-1} stretches, the calculation predicts $\nu_1 = 119$ cm^{-1} ($\Delta\nu^{16,18} = -1.4$). The results using both sets of experimental frequencies are given in Table 3.

When the core metrical parameters for the L^{TMPD} dimer are input ($r_{\text{Cu}\cdots\text{Cu}} = 2.85$ Å, $r_{\text{Cu}-\text{O}} = 1.81$ Å; $r_{\text{O}\cdots\text{O}} = 2.23$ Å),[11] the NCA predicts values of $\nu_3 = 607.0$ cm^{-1} and $\nu_1 = 134.6$ cm^{-1}, which correlate well with the experimental values for this complex of 609 and 133 cm^{-1}, respectively. The observed shift in frequency of ν_1 from 118 to 133 cm^{-1} is therefore due to a change in the core geometry (resulting from an increase in metal

coordination number from 4 to 5, *vide supra*) rather than mixing of amine ligand character into this mode. Thus, despite the change in ν_1 with ligand variation, this mode is well-characterized using only Cu$_2$O$_2$ motion.

Quantitative illustrations of the calculated modes are given in Figure 7. Since out-of-plane motion is disregarded, five in-plane modes are calculated from the $3N - 6 = 6$ degrees of freedom for the Cu$_2$O$_2$ unit. Of these, two modes are totally symmetric Raman-active a$_g$ modes (ν_1 and ν_3). Both their calculated frequencies and isotope shifts agree well with the experimental data. As shown in Table 2, the observed range of frequencies for $\nu_s(\text{Cu}-\text{O})$ (i.e., ν_3) is 605−616 cm^{-1} ($\Delta\nu^{16,18} = -23$ to -28). The computed value of 611.5 cm^{-1} ($\Delta\nu^{16,18} = -28.1$) falls well within this range. The difference between the calculated value of $\nu_1 = 118.6$ cm^{-1} and the experimental value of 118 cm^{-1}, as well as its small calculated isotope shift of $\Delta\nu = -1.4$ cm^{-1}, both fall within the experimental error of the rR experiment. Note that the Cu−O bond strength, as indicated by its force constant $k_{\text{Cu}-\text{O}} = 2.699$ mdyne/Å, is high relative to previous normal coordinate analyses performed on the Cu(II)$_2$ side-on peroxo-bridged dimer (for which $k_{\text{Cu}-\text{O}} = 1.42$ to 1.72).[37] This shows good agreement with the Cu(III)$_2(\mu\text{-}O^{2-})_2$ electronic structural description of the bis-μ-oxo dimers.

The NCA-derived mass-weighted eigenvectors l_i for the n normal modes used in calculating the excited-state geometry (*vide infra*) are given in Table 3.
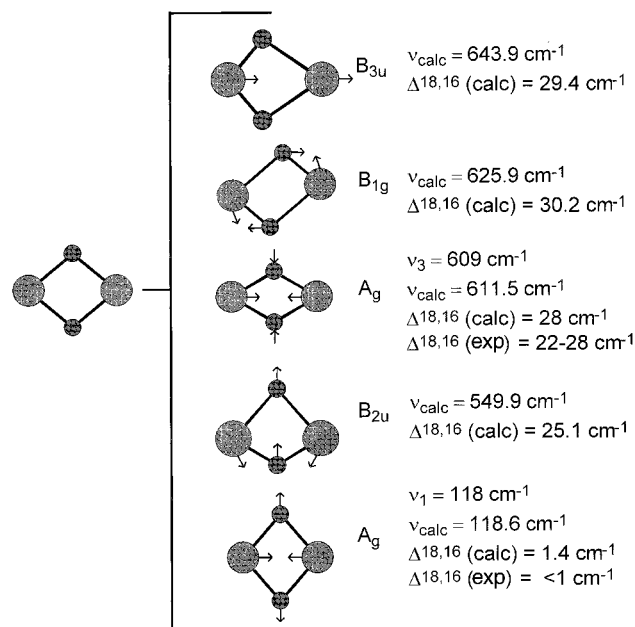
Figure 7. Normal modes of vibration for the D_{2h} Cu_2O_2 core from a normal coordinate analysis. Only the two a_g modes at 611.5 and 118.6 cm^{-1} are Raman-active.

D. Excited-State Geometry from Profiles and Overtones. For a quantitative analysis of the resonance Raman (rR) profiles collected for the L^{MECHD} bis-μ-oxo dimer, an intensity correction is needed for the profile for the $\nu_1 = 118$ cm^{-1} mode to account for the thermal population of the first vibrational excited state at the experimental temperature of 193 K. Approximately 40% of dimer molecules should be in Boltzmann-populated excited ($\nu > 0$) vibrational states at $T = 193$ K. Einstein coefficients predict equal probabilities of ($\Delta\nu = -1$ and $+1$) transitions from these excited levels. This results in approximately 20% of sample molecules undergoing anti-Stokes ($\Delta\nu = -1$) transitions and a total of 80% undergoing Stokes ($\Delta\nu = +1$) transitions. The probabilities of a Stokes transition originating out of the excited versus ground vibrational levels was derived using the equation for the rR cross section for each transition[15c]

$$\sigma_{i \rightarrow f} = 5.87 \times 10^{-19} M^4 E_S^3 E_L \left| \sum_\nu \frac{\langle f|\nu\rangle\langle\nu|i\rangle}{\epsilon_\nu - \epsilon_i + E_0 - E_L - i\Gamma} \right|^2 \tag{1}$$

where E_0 is the energy of the transition between the lowest vibrational levels of the ground and excited electronic states, E_L is the laser excitation energy, E_S is the energy of the scattered photon, M is the electronic transition dipole vector, Γ is a damping factor, and $\langle f|\nu\rangle$ and $\langle\nu|i\rangle$ are the vibrational overlap integrals between two distorted electronic surfaces. The vibrational overlap integrals were computed as a function of the Hermite polynomials[38] and the dimensionless excited-state distortion parameter, Δ, in the form of the Huang−Rhys parameter[39] $S (= \Delta^2/2)$

Table 4

	$\nu/$ cm^{-1}	relative $|\Delta|$	exp. fit	$\Delta r_{Cu-O}/$Å	$\Delta r_{O-O}/$Å
ν_1	118	2.7−4.1	+5.4	+0.0286 ± 0.0016	−0.450 ± 0.025
ν_2	476	≪1			
ν_3	609	1.00	+2.0	+0.0625 ± 0.0031	+0.1493 ± 0.0074
ν_4	827	0.33			
ν_5	950	0.27			
total distortion:				+0.091 ± 0.005	−0.301 ± 0.017

$$\langle\chi_{bn}|\chi_{am}\rangle = \exp\left(\frac{-S}{2}\right)\left[\frac{m!}{n!}\right]^{1/2}(S)^{(n-m)/2}L_m^{n-m}(S) \tag{2}$$

where χ_{am} and χ_{bn} are the initial and final vibrational levels of the a and b electronic states and $L_m^{n-m}(S)$ is the Langmuir polynomial. Plugging eq 2 into eq 1 allows calculation of the excitation profiles for the Stokes transitions originating out of both the vibrational ground and excited states. Comparison of the theoretical profile intensities at $T = 0$ and 193 K shows that approximately 18% ($\pm 2\%$)[40] of the rR intensity for ν_1 was lost due to anti-Stokes transitions. Therefore the rR profile for $\nu_1 = 118$ cm^{-1} was scaled by 1.22 to compensate for this thermal intensity loss.

Comparison of the rR peak intensity ratios gives important information about the relative magnitudes of the excited-state distortions along each mode. Using eq 3,[15d,41] the Δ's for the L^{MECHD} rR modes which showed resonance enhancement were calculated relative to that of ν_3 (Table 4).

$$\frac{I_k}{I_{k'}} = \frac{(\Delta_k^2 \nu_k^2)}{(\Delta_{k'}^2 \nu_{k'}^2)} \tag{3}$$

I_k is the integrated Raman peak intensity for the mode with frequency ν_k in the preresonance region ($E_0 > E_L$). The small distortions predicted for the ν_2, ν_4, and ν_5 amine ligand-type modes relative to the core modes ν_1 and ν_3 confirms that they may be excluded in the analysis of excited-state distortions developed below.

Time-dependent Heller theory[15] was employed to simultaneously fit both the rR profiles of ν_1 and ν_3 and the absorption spectrum of the L^{MECHD} dimer. The ($\Delta_{118}/\Delta_{609}$) ratio results from the fit of the rR profiles, while the absolute magnitudes of Δ_{118} and Δ_{609} were obtained by the simultaneous fit of the calculated absorption band to the 25 000 cm^{-1} charge-transfer feature. This analysis (Figure 8) results in values of $|\Delta_{609}| = 2.0 \pm 0.1$ and $|\Delta_{118}| = 5.4 \pm 0.3$.

The experimental overtone progressions for these two modes give the signs of the corresponding Δ's (the directions of the excited-state distortions). Morris and Woodruff[42] show that a decrease in the overtone/fundamental intensity ratio with increasing excitation energy indicates a decreased force constant in the excited state. Provided Badger's rule[43] is obeyed, this

(37) (a) Baldwin, M. J.; Root, D. E.; Pate, J. E.; Fujisawa, K.; Kitajima, N.; Solomon, E. I. *J. Am. Chem. Soc.* **1992**, *114*, 10421−10431. (b) Ling, J.; Nestor, L. P.; Czernuszewicz, R. S.; Spiro, T. G.; Fraczkiewicz, R.; Sharma, K. D.; Loehr, T. M.; Sanders-Loher, J. *J. Am. Chem. Soc.* **1994**, *116*, 7682−7691.

(38) (a) Fitchen, D. B. In *Physics of Color Centers*; Fowler, W. B., Ed.; Academic Press: New York, 1968; pp 293−350. (b) Keil, T. H. *Phys. Rev.* **1965**, *140*, A601−617.

(39) Huang, K.; Rhys, A. *Proc. R. Soc. London, A* **1951**, *208*, 352.

(40) The uncertainty in the % intensity loss is due to inclusion of a wide range of possible values of Δ_{118} in the calculation. Prior to thermal renormalization of the rRaman peak intensity for ν_1, time-dependent Heller theory fits of the rR profiles and absorption spectrum had given: $|\Delta_{118}| = 5.00$; $|\Delta_{609}| = 1.90$. Allowing Δ_{118} to vary over a larger range (3.0−6.0) resulted in a highly reproducible ratio of profile intensity at $T = 193$ K relative to that at $T = 0$ K of 0.82 ± 0.02.

(41) (a) Tang, J.; Albrecht, A. C. In *Raman Spectroscopy*; Szynaski, H., Ed.; Plenum Press: New York, 1970; Vol. 2, p 33. (b) Warshel, A.; Dauber, P. *J. Chem. Phys.* **1977**, *66*, 5477.

(42) Morris, D. E.; Woodruff, W. H. *J. Phys. Chem.* **1985**, *89*, 5795−5798.

(43) Badger, R. M. *J. Chem. Phys.* **1934**, *2*, 128−131.
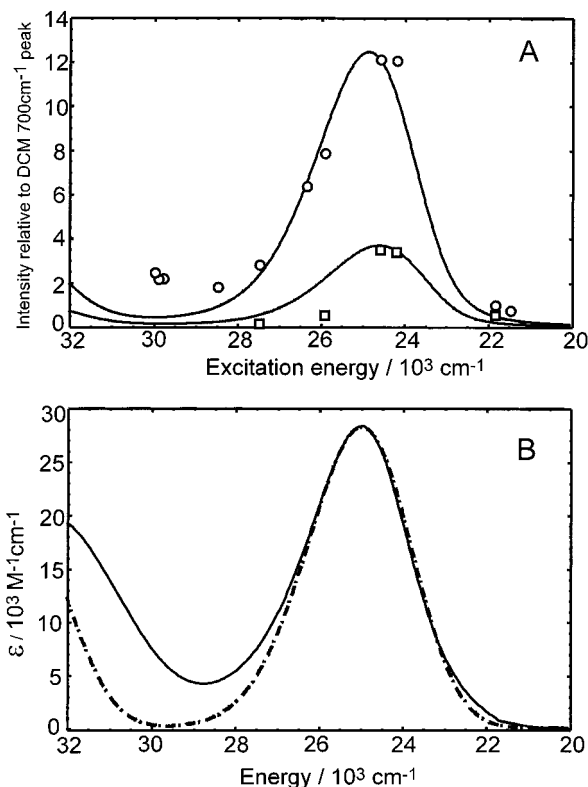
Figure 8. (a) Time-dependent Heller theory[15] fits (solid lines) of the $\nu_1 = 118$ cm^{-1} ($\square$) and $\nu_3 = 609$ cm^{-1} ($\bigcirc$) resonance Raman excitation profiles, and (b) the simultaneous fit (broken line) of the electronic absorption spectrum (solid line) using the dimensionless excited-state distortion parameters $|\Delta_{118}| = 5.4$ and $|\Delta_{609}| = 2.0$.

allows assignment of the direction of the excited-state distortion. The ratio of the excitation profile of $2\nu_3 = 1218$ cm^{-1} to that of $\nu_3 = 609$ cm^{-1} (Figure 6, inset) shows a clear negative slope with increasing E_L (decreasing λ_{ex}). The direction of this trend arises from a weaker modal force constant in the excited state, which results in increased Cu–O bond lengths and $\Delta_{609} > 0$. Data collected for two different bis-μ-oxo dimers also allow determination of the direction of distortion along $\nu_1 = 118$ cm^{-1}. The first overtone of ν_1, $2\nu_1 = 236$ cm^{-1}, was observed in the L^{MECHD} spectra collected for $\lambda_{ex} = 413.1$ and 406.7 nm. The first and second overtones for the L^{TMPD} dimer, $2\nu_1 = 266$ and $3\nu_1 = 399$ cm^{-1}, were also observed at these two excitation energies. The intensity ratios of the overtones to the fundamentals for these dimers (Figure S2) are both less for the high-energy line (406.7 nm = 24 588 cm^{-1}) than for the lower-energy line (413.1 nm = 24207 cm^{-1}). This trend is supported by the lack of observable overtones relative to baseline noise at the next available laser line (385.8 nm = 25 920 cm^{-1}). The direction of this trend indicates that Δ_{118} is also positive, corresponding to a lengthened Cu–O bond and a decrease in the O⋯O separation in the CT excited state.[44]

The dimensionless Δ_n is related to the dimensioned distortion ΔQ_n (in Å) along the normal mode Q_n by the following relationship:

$$\Delta Q_n = \frac{5.8065}{\sqrt{\mu_n \nu_n}} \tag{4}$$

---

(44) Although the potential energy distribution (PED) for $\nu_1 = 118$ cm^{-1} indicates that O–O motion dominates (86.4%) the modal energy, the bonding interaction which dominates the Cu$_2$O$_2$ core is Cu–O. Therefore $\Delta_{118} > 0$ corresponds to $\Delta r_{Cu–O} > 0$ (and thus $\Delta r_{O⋯O} < 0$).

where μ_n is the molar reduced mass and ν_n the frequency of normal mode Q_n. Combination of the signed Δ_n's with the mass-weighted eigenvectors from the NCA allows determination of the actual bond length changes associated with the excited-state distortion[15c]

$$\Delta r_i(\text{Å}) = \sum_n (l_{n,i}\sqrt{\mu_n})\Delta Q_n = 5.8065 \sum_n l_{n,i} \frac{\Delta_n}{\sqrt{\nu_n}} \tag{5}$$

The distortions along each coordinate for ν_1 and ν_3, as well as the resulting net excited-state distortion are given in Table 4. The net change in the Cu–O bond length due to the electronic transition associated with the 25 000 cm^{-1} CT absorption feature is +0.091 Å. The positive distortion indicates a lengthening of the Cu–O bond. This is consistent with the description of this transition as an oxo-to-Cu(III) LMCT. Interestingly, a large simultaneous shortening (−0.301 Å) of the O⋯O separation occurs upon excitation. The origin of this change in bonding can be understood in terms of the assignment for the 25 000 cm^{-1} CT, based on electronic structure calculations presented below.

E. Electronic Structure Calculations. A structural model derived from the crystallographic coordinates of the L^{MECHD} bis-μ-oxo dimer was used as input for all electronic structural calculations. The substituted diamine ligands were truncated to simple NH$_3$ ligands. The near-D_2 symmetry of the crystal structure was idealized to D_{2h} by shifting the nitrogens into the Cu$_2$O$_2$ plane while preserving the average experimental Cu–N bond length. The idealized D_{2h} metrical parameters of the core were: Cu⋯Cu = 2.73 Å, O⋯O = 2.34 Å, and Cu–O = 1.80 Å. The input coordinates are included in the Supporting Information (Table SM1), with a molecular coordinate frame in which the Cu–Cu vector lies along the x-axis and the O–O vector along the y-axis. The results of the SCF Xα-SW[22-27] calculation for the bis-μ-oxo model with a Cu sphere radius of 2.75 bohr are presented in Table 5. The molecular orbital energy diagram is shown in Figure 9, with electron density contour plots included for MO's of particular interest.

From the Slater transition-state calculations (Table 6), three transitions are possible within the correct energy range and with the proper orbital composition to give rise to the intense $\Delta E = 25\,000$ cm^{-1} oxo-to-Cu(III) CT. Possible transitions into both the 11B$_{3u}$ LUMO and the 9B$_{2g}$ LUMO+1 are considered, as only 2000 cm^{-1} separates these orbitals in the calculation (compared to the $\Delta E > 8000$ cm^{-1} HOMO/LUMO splitting). These acceptor orbitals are primarily Cu d$_{xy}$ in character,[3] indicating that the two lowest-energy holes are primarily metal-based, consistent with the assigned +3 oxidation state. This oxidation state is stabilized by a large degree of Cu–oxygen covalency, which serves to partially delocalize the holes (MO's 11B$_{3u}$ and 9B$_{2g}$ in Table 5) onto the oxo ligands. The potential CT assignments considered here exclude the symmetry-allowed, lower-energy transitions from the 5B$_{1g}$ ("π_ν*") or 5B$_{2u}$ ("π_ν^b") donors.[45] These MO's are composed of the bonding and antibonding combinations of the oxygen p$_z$ orbitals which are perpendicular to the Cu$_2$O$_2$ plane. These orbitals have no overlap

---

(45) The bonding and antibonding combinations of the oxygen p-orbitals in the bis-μ-oxo model will be referred to by the D_{8h} Mulliken symbols (σ_g, σ_u*, $\pi_{\nu,\sigma}^b$, $\pi_{\nu,\sigma}$*,...) which are typically used to label the O$_2$ molecular orbitals. This makes for ease of reference and correlation to the side-on peroxo model in which these symbols are used to describe MO composition. There is of course no O–O bond in the bis-μ-oxo structure.

Table 5[a]

level	occ	E/eV	% Cu	% O	% N	Cu d-orbital(s)	O p-orbitals
9 B$_{2G}$ (LUMO+1)	0	−4.001	58	22	18	$xy(+)$	p$_x$−p$_x$ ("π_σ*")
11 B$_{3U}$ (LUMO)	0	−4.257	56	31	12	$xy(-)$	p$_y$+p$_y$ ("σ_u*")
5 B$_{1G}$	2	−5.258	25	75	0		p$_z$−p$_z$ ("π_v*")
5 B$_{2U}$	2	−5.875	41	58	0		p$_z$+p$_z$ ("π_v^{b}")
12 A$_G$	2	−6.891	72	27	0	$x^2-y^2(+)$	p$_y$−p$_y$ ("σ_g")
10 B$_{1U}$	2	−7.327	89	10	1	$x^2-y^2(-)$, $z^2(-)$	p$_x$+p$_x$ ("π_σ^{b}")
9 B$_{3U}$	2	−7.486	27	51	20	$xy(-)$	"σ_u*"
11 A$_G$	2	−7.755	90	1	8		
9 B$_{1U}$	2	−7.866	95	1	3		
3 B$_{3G}$	2	−8.000	99	0	0		
3 A$_U$	2	−8.108	99	0	0		
3 B$_{1G}$	2	−8.545	86	13	0		
3 B$_{2U}$	2	−8.945	78	21	0		
7 B$_{1U}$	2	−9.260	34	27	35	$x^2-y^2(-)$, $z^2(-)$	"π_σ^{b}"
7 B$_{2G}$	2	−9.704	33	19	43	$xy(+)$	"π_σ*"
9 A$_G$	2	−10.062	45	26	25	$x^2-y^2(+)$, $z^2(+)$	"σ_g"
7 A$_G$	2	−10.449	44	24	28	$x^2-y^2(+)$	"σ_g"
7 B$_{3U}$	2	−10.491	52	6	38	$xy(-)$	
5 B$_{1U}$	2	−11.434	48	33	17	$x^2-y^2(-)$, $z^2(-)$	"π_σ^{b}"
5 B$_{2G}$	2	−11.617	58	36	5	$xy(+)$	"π_σ*"

[a] Cu sphere radius = 2.75 bohr.
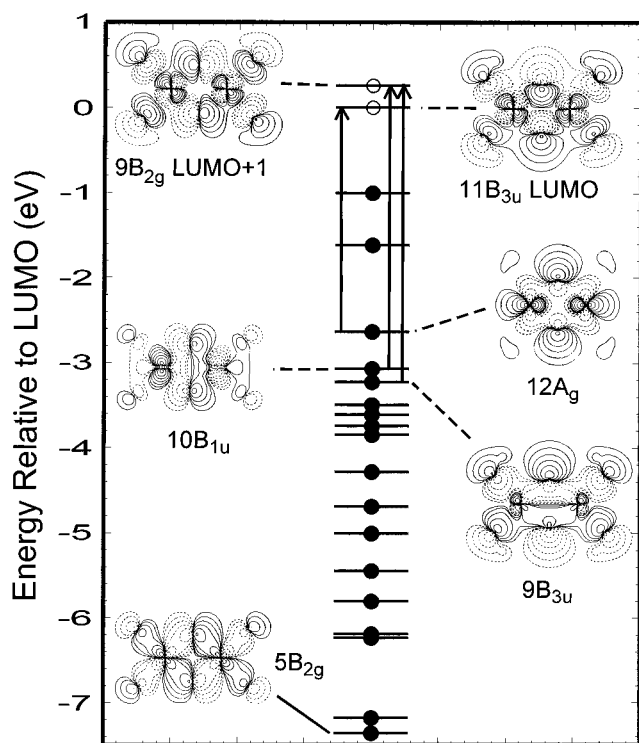
Figure 9. SCF Xα-SW molecular orbital energy digram showing the three possible assignments (arrows) for the 25 000 cm^{-1} charge-transfer transition. Contours of the donor and acceptor orbitals are shown, as well as the deep-energy Cu(III) d$_{xy}$/oxo π_σ* bonding orbital (5B$_{2g}$).

with the acceptor molecular orbitals and thus cannot give rise to intense charge-transfer transitions. The allowed transitions (Table 6, Figure 9) each exhibit either nonzero ligand–ligand or metal–metal overlap with the 11B$_{3u}$ (LUMO) and the 9B$_{2g}$ (LUMO+1) acceptor orbitals. The 12A$_g$ MO is primarily an antibonding interaction between the positive combination of Cu d$_{x^2-y^2}$ orbitals and the oxygen p$_y$−p$_y$ bonding orbital, σ_g (note: the y-axis is the O−O vector). The 10B$_{1u}$ MO is the antibonding interaction between the negative combination of the Cu d$_{x^2-y^2}$ orbitals with the oxygen p$_x$+p$_x$ bonding orbital, π_σ^{b}. Unlike these donor possibilities, the 9B$_{3u}$ MO is a *bonding* interaction between the negative combination of Cu d$_{xy}$ orbitals and the

oxygen p$_y$+p$_y$ antibonding orbital, σ_u*. This MO is qualitatively similar in composition to the HOMO of the side-on peroxo dimer. However, the stabilization of the antibonding σ_u* upon lengthening of the O···O distance from 1.41 to 2.34 Å results in both a corresponding energetic stabilization of the 9B$_{3u}$ MO, enough that it may now be considered as a viable CT donor possibility, and an increased oxygen contribution to the wave function (from < 2% in the side-on peroxo to approximately 48% in the bis-μ-oxo). This stabilization of the 9B$_{3u}$ is the electronic origin of the O−O bond cleavage in the bis-μ-oxo model: increased donation of electron density from the Cu's into the dioxygen σ-antibonding orbital leads to the Cu(III)$_2$ bis-μ-oxo structure.

SCF Xα-SW calculations have previously been used to predict the direction of the excited-state distortions (signs of Δ's) for a series of possible charge-transfer transitions along different vibrational modes.[46] Slater transition-state calculations were performed on geometries obtained from the ground-state coordinates by imposing small positive and negative distortions, ΔQ, along the two a$_g$ normal modes. The geometric dependence of the charge-transfer energies can be described as a linear electron–nuclear coupling term in the excited state relative to the ground state[46,47]

$$E_{ele-nuc} \equiv \langle \psi_{ex} | (\partial \hat{V}_{ex}/\partial Q)_0 | \psi_{ex} \rangle \times Q \qquad (6)$$

Determination of the Slater transition energies in the limit of small geometric perturbations, $(\Delta E^{X\alpha}/\Delta Q)_0$, gives an approximation to the electronic coupling matrix element in eq 6, assuming that the Xα-SW ground-state potential is at a minimum in the experimentally observed ground-state equilibrium geometry. The sign of this coupling term for a charge-transfer transition gives the direction of the excited-state distortion corresponding to that transition. Additionally, the size of this quantity can be used to approximate the relative magnitudes of the distortions which would result from the different transitions.

(46) Gamelin, D. R.; Bominaar, E. L.; Mathonière, C.; Kirk, M. L.; Wieghardt, K.; Girerd, J.,-J.; Solomon, E. I. *Inorg. Chem.* **1996**, *35*, 4323−4335.

(47) Solomon, E. I. *Comments Inorg. Chem.* **1984**, *3*, 227−320.

Table 6

	ΔE_{Slater}	relative f_{calc}	$\Delta E_{609+}{}^a$	$\Delta E_{609-}{}^a$	$\Delta E_{118+}{}^b$	$\Delta E_{118-}{}^b$	rel. ΔQ_{609}	rel. ΔQ_{118}
			Xa (Cu Sphere Radius = 2.65 Bohr)					
$12A_g \rightarrow 11B_{3u}$	23 317	0.778	+137.1	−153.3	−548.5	+798.4	−1.19	+6.96
$10B_{1u} \rightarrow 9B_{2g}$	29 504	0.353	−129.0	+88.7	+556.5	−1322.7	+1.00	−16.8
$9B_{3u} \rightarrow 9B_{2g}$	30 092	1.000	−129.1	+145.2	−1927.7	+1742.1	+1.00	+24.5

	ΔE_{Slater}	relative f_{calc}			$\Delta E_{118+}{}^c$	$\Delta E_{118-}{}^c$		rel. ΔQ_{118}
			Xa (Cu Sphere Radius = 2.75 Bohr)					
$12A_g \rightarrow 11B_{3u}$	21 382	0.472			−112.9	+1056.6		+0.96
$10B_{1u} \rightarrow 9B_{2g}$	27 399	0.175			+790.4	−1371.1		−11.6
$9B_{3u} \rightarrow 9B_{2g}$	29 310	1.000			−2798.7	+2185.8		+23.7

$^a \Delta Q_{609} = \pm 0.0325$ Å ($\Delta_{609} = \pm 0.333$). $^b \Delta Q_{118} = \pm 0.0753$ Å ($\Delta_{118} = \pm 0.900$). $^c \Delta Q_{118} = \pm 0.113$ Å ($\Delta_{118} = \pm 1.35$).

$$\Delta Q_n = -\frac{\left\langle \psi_e^{ele} \left| \left(\frac{\partial \hat{V}_{ex}}{\partial Q_n}\right)_0 \right| \psi_e^{ele} \right\rangle}{k_n} \tag{7}$$

The predicted excited-state distortion directions for the different possible assignments of the 25 000 cm⁻¹ band are given in Table 6. The $12A_g \rightarrow 11B_{3u}$ transition gives $\Delta_{609}(-)$ and $\Delta_{118}(+)$. The $10B_{1u} \rightarrow 9B_{2g}$ transition gives $\Delta_{609}(+)$ and $\Delta_{118}(-)$. Only the $9B_{3u} \rightarrow 9B_{2g}$ transition gives predicted distortional directions in agreement with those observed experimentally: $\Delta_{609}(+)$ and $\Delta_{118}(+)$. These distortional directions may be rationalized as follows. The B_{1u} and B_{3u} donors transfer electron density into the B_{2g} LUMO+1 (Figure 9). This acceptor MO has a stronger Cu/O antibonding interaction than in the B_{1u} donor, favoring a positive distortion along the $\nu_3 = 609$ cm⁻¹ mode. As the $9B_{3u}$ is a Cu/O bonding orbital, charge transfer to a Cu/O antibonding orbital will clearly result in a positive excited-state distortion for the low-frequency mode, ν_1. The B_{1u} to B_{2g} transition is between an O−O π-bonding MO and an O−O π-antibonding MO, favoring a lengthened O···O separation in the excited state and thus $\Delta_{118} < 0$ (ref. 44), while the B_{3u} to B_{2g} transition involves a O−O σ-antibonding MO to a O−O π-antibonding MO transition, favoring a shorter O−O distance in the E.S., giving $\Delta_{118} > 0$. For the $12A_g \rightarrow 11B_{3u}$ transition, there are opposing forces involved in the distortions due to this transition which depend on the covalency of the model used.[48] However, the magnitudes of the distortions predicted for this transition rule it out as a possible assignment. Experimentally, a larger distortion is observed along the 118 cm⁻¹ relative to the 609 cm⁻¹ mode ($\Delta_{118} = +5.4$, $\Delta_{609} = +2.0$). As shown in Table 6, the $9B_{3u} \rightarrow 9B_{2g}$ transition is predicted to have the largest distortion along the low-frequency a_g ($\nu_1 = 118$ cm⁻¹) mode. Therefore, only the $9B_{3u} \rightarrow 9B_{2g}$ transition has the correct distortional directions and magnitudes for assignment as the 25 000 cm⁻¹ CT band.

The relative charge-transfer intensities (oscillator strengths) are also consistent with the assignment of the 25 000 cm⁻¹ band as the $9B_{3u} \rightarrow 9B_{2g}$ transition. The results of the Xα calculations for several values of the Cu sphere radius are given in Table 6. Theoretical oscillator strengths were computed from the Xα wave function using the Ros−van der Avoird method.[49] Comparative values were also obtained using the INDO/S (semiempirical ab initio + CI with 60 000 states) method (see refs 50 and 51). The nature of the orbital overlap integrals

Table 7

transition	Cu S. R. = 2.65 bohr		Cu S. R. = 2.75 bohr	
	ΔE_{Slater}	relative f_{calc}	ΔE_{Slater}	relative f_{calc}
$7B_{1u}$ to $9B_{2g}$ (LUMO+1)	42142	0.0710	43884	0.0759
$7B_{2g}$ to $11B_{3u}$ (LUMO)	44102	0.0432	45570	0.0462
$9A_g$ to $11B_{3u}$	47772	0.0395	47377	0.1017
$7A_g$ to $11B_{3u}$	51555	0.1575	50692	0.0885
$5B_{2g}$ to $11B_{3u}$	59894	1.0000	59419	1.0000
$5B_{1u}$ to $9B_{2g}$	61451	0.1347	60604	0.1262

between the donor and acceptor MO's for the three transitions varies greatly. The A_g and B_{1u} donors have poor metal/metal (MM) overlap with their respective acceptors since both involve $d_{x^2-y^2}$ to d_{xy} transitions. However, these transitions will have significant ligand/ligand (LL) overlap. On the other hand, the $9B_{3u}$ transition to $9B_{2g}$ has very good MM overlap (d_{xy} to d_{xy}) but no LL overlap. These differences indicate that the calculated relative oscillator strengths depend strongly upon the covalency of the model employed. Increasing covalency in the calculations will tend to increase the LL overlap at the expense of the MM overlap. Within the sphere radius range of 2.65−2.75 bohr which best describes the Cu(III)₂ bis-μ-oxo core relative to experiment, the most intense transition is predicted to be $9B_{3u} \rightarrow 9B_{2g}$. The INDO/S calculation, which overestimates all of the transition energies, predicts that the CT transition originating from the B_{3u} MO would be approximately 40 times as intense as the transition originating from the A_g and more than 5000 times as the $10B_{1u} \rightarrow 9B_{2g}$ transition.[50] The agreement in relative intensities between two methods supports the assignment of the $E_1 = 25\,000$ cm⁻¹ CT as the $9B_{3u}$ (d_{xy}/σ_u^* bonding) to $9B_{2g}$ (d_{xy}/π_σ^* antibonding) transition.

The absorption spectrum for the L^{MECHD} bis-μ-oxo dimer also exhibits a high-energy (32 700 cm⁻¹) charge-transfer band of similarly large intensity ($\epsilon = 21\,000$ M⁻¹ cm⁻¹) to the lower-energy CT feature. The SCF Xα-SW calculation predicts a number of possible deep binding energy donor MO's for this higher-energy transition (Table 5). The calculated oscillator strengths for these transitions are given in Table 7. The $5B_{2g}$ to $11B_{3u}$ transition is predicted to be approximately 6 times more

(48) Increasing the Cu-ligand covalency in the Xα calculation by decreasing the Cu sphere radius results in the direction of the predicted distortion along this mode changing from positive to negative. Decreasing the covalency of the model reduces the importance of stabilization due to changes in Cu−O bonding, resulting in the direction of the excited-state distortion along this mode being determined by changes in O−O bonding.

(49) Van der Avoird, A.; Ros, P. *Theor. Chim. Acta* **1966**, *4*, 13-21.

(50) Orca is a program written by Dr. Frank Neese that was used to perform the semi-empirical INDO/S calculations (ref 50x): $E(12A_g \rightarrow 11B_{3u}) = 30,791$ cm⁻¹, relative $f_{osc} = 0.024$; $E(9B_{3u} \rightarrow 9B_{2g}) = 38,614$ cm⁻¹, rel. $f_{osc} = 1.000$. The $10B_{1u} \rightarrow 9B_{2g}$ transition was not calculated as a CT of significant intensity, thus we approximate rel $f_{osc} = 0.000$.

(51) (a) Ridley, J.; Zerner, M. C. *Theor. Chim. Acta* **1973**, *32*, 111. (b) Bacon, M. D.; Zerner, M. C. *Theor. Chim. Acta* **1979**, *53*, 21. (c) Zerner, M. C.; Loew, G. H.; Kirchner, R. F.; Mueller-Westerhoff, U. T. *J. Am. Chem. Soc.* **1980**, *102*, 589. (d) Anderson, W. P.; Edwards, W. D.; Zerner, M. C. *Inorg. Chem.* **1986**, *25*, 2728.

Table 8

Cu S. R. = 2.75 au	D_{2h} CHD	C_{2h} TACN
σ_g (12A$_g$) to LUMO (11B$_{3u}$)	21 383	21 115 (−267)
π_σb (10B$_{1u}$) to LUMO+1 (9B$_{2g}$)	27 399	39 376 (+12000)
σ_u* (9B$_{3u}$) to LUMO+	29 310	27 124 (−2168)
π_σ* (5B$_{2g}$) to LUMO	59 419	55 870 (−3549)
Cu S. R. = 2.65 au		
σ_g to LUMO	23 317	
π_σb to LUMO+1	29 504	
σ_u* to LUMO+1	30 092	27 858 (−2234)
π_σ* to LUMO	59 894	
E_1 (exp.)	32 000− 34 500	30 800−31 400 (−700 to −2900)
E_2 (exp.)	24 600− 25 700	22 300−23 300 (−1300 to −3200)

intense than any other of the transition possibilities. As shown in Figure 9, the 5B$_{2g}$ MO is a bonding interaction between the oxygen p$_x$ orbitals (π_σ*) and the positive combination of Cu d$_{xy}$ orbitals. Although the Xα calculation overestimates the CT transition energy by almost a factor of 2, a reasonable energetic and intensity correlation exists between this feature (E_{exp} = 32 700 cm^{-1}, ϵ = 21 000 M^{-1} cm^{-1}) and a similar band in the absorption spectrum of the side-on peroxo-bridged μ-η^2:η^2 complex (E_{exp} = 28 600 cm^{-1}, ϵ = 20 000 M^{-1} cm^{-1}).[1] This band in the side-on peroxo dimer spectrum was assigned as a peroxo π_σ* (B$_{2g}$) to Cu(II) d$_{xy}$ LUMO LMCT.[4] The shift of this band to higher energy would reflect the stabilization of the d$_{xy}$/π_σ* bonding orbital due to an increase strength of the Cu−O bonding interaction for the Cu(III)$_2$(μ-O^{2-})$_2$ dimer relative to Cu(II)$_2$(μ-O$_2^{2-}$) as well as a reduction in the O/O π* interaction with increased O···O separation.

The CT transition energies were calculated for both the 4-coordinate (D_{2h}) bis-μ-oxo model as well as a 5-coordinate (C_{2h}) model based upon coordinates reported by Tolman for the L^{Bn_3TACN} dimer.[52] For the three possible assignments previously discussed for the 25 000 cm^{-1} CT transition, only the 9B$_{3u}$ (σ_u*) to 9B$_{2g}$ (d$_{xy}$) transition reproduces the experimental trend between the 4- and 5-coordinate dimers (Table 8). This transition is calculated to shift 2168 cm^{-1} lower in energy in the 5- relative to the 4-coordinate model, which is in good agreement with the experimental shift (Table 1) of between −800 (L^{Me_3TACN} vs L^{TMCHD}) and −3200 cm^{-1} (L^{iPr_3TACN} vs L^{TMCHD}) for this band upon an increase in coordination number (CN). In contrast, the other two possible assignments, 10B$_{1u}$ (π_σb) to 9B$_{2g}$ and 12A$_g$ (σ_g) to 11B$_{3u}$ (d$_{xy}$), show corresponding shifts of +12 000 and −270 cm^{-1}, respectively. Similarly, the 5B$_{2g}$ (π_σ*) to 11B$_{3u}$ transition shows a shift to lower energy upon CN increase (−3550 cm^{-1}) that is close to the experimental shift of the higher-energy CT at 32 700 cm^{-1} by an amount between −700 (L^{Me_3TACN} vs L^{TMCHD}) and −3100 cm^{-1} (L^{iPr_3TACN} vs L^{TMCHD}). The consistency of these calculated shifts with experimental results provides further support for our CT assignments.

Further, separate calculations were performed to evaluate the relative contributions to these CT transition energy shifts from increases in metal CN and metal−metal distance. The 9B$_{3u}$ to 9B$_{2g}$ transition energy was affected predominantly by the Cu$_2$O$_2$ core geometry, while the 5B$_{2g}$ to 11B$_{3u}$ transition energy was influenced more by the addition of a fifth ligand, which is consistent with the nature of the above assignments.

(52) Mahapatra, S.; Halfen, J. A.; Wilkinson, E. C.; Pan, G.; Cramer, C. J.; Que, L., Jr.; Tolman, W. B. *J. Am. Chem. Soc.* **1995**, *117*, 8865−8866.

Discussion

Description of Cu$_2$O$_2$ Bonding. The electronic description of the Cu(III)$_2$ bis-μ-oxo dimers previously obtained from XAS results[9,11] is further supported by the present spectroscopic studies. The force constants from the resonance Raman-based normal coordinate analysis are indicative of increased Cu−O (k_{Cu-O} = 2.699 mdyne/Å) and greatly reduced O−O (k_{O-O} = 0.297 mdyne/Å) bond strengths relative to the Cu(II) side-on peroxo-bridged dimer (k_{Cu-O} = 1.42−1.72, k_{O-O} = 1.41−1.45 mdyne/Å).[37] These changes in bond strengths are consistent with the short Cu−O (1.80 Å) bonds and the large O···O (2.34 Å) separation in the X-ray crystal structure of the [(L^{MECHD}Cu)$_2$-(μ-O^{2-})$_2$]$^{2+}$ dimer.[8] The absorption spectrum of the L^{MECHD} dimer is characterized by two intense charge-transfer features at 32 700 cm^{-1} (21 000 M^{-1} cm^{-1}) and 25 000 cm^{-1} (28 000 M^{-1} cm^{-1}). The higher-energy feature correlates well with the energy and intensity of a band in the side-on peroxo absorption spectrum (E_{exp} = 28 600 cm^{-1}, ϵ = 20 000 M^{-1} cm^{-1}) which was previously assigned as a peroxo π_σ* to Cu(II) CT transition and has a similar assignment in the bis-μ-oxo structure (*vide supra*). Since CT energy and intensity quantitate the L-donor interaction with the metal, the origin of the increased Cu−O bonding interaction relative to the side-on peroxo dimer is reflected in the new, intense, low-energy charge-transfer absorption feature at 20 000−26 000 cm^{-1} for the bis-μ-oxo dimer. This band indicates the presence of a new donor orbital. The large Raman enhancement of the Cu$_2$O$_2$ symmetric core stretch at ν = 609 cm^{-1} when in resonance with this band is consistent with assignment as an oxo to Cu(III) CT and indicates that a large excited-state distortion results from this charge transfer. The excited-state distortion is determined to involve a Cu−O bond length change of +0.09 Å (from 1.80 to 1.89 Å) and a change in O···O separation of −0.30 Å (from 2.34 to 2.03 Å) (see ahead to Figure 11, top two structures), consistent with this oxo to Cu(III) CT transition producing an excited state which formally has Cu(II)-oxyl character. The intensity of this CT transition indicates a high degree of metal−ligand covalency.

Electronic structure calculations allow assignment of this CT feature as an oxo σ_u* (ref 45) to Cu d$_{xy}$ transition. This is the only transition which will give the expected absorption intensity as well as the direction and magnitude determined for the excited-state distortion. A shift of the O$_2^{2-}$ σ_u* high-energy unoccupied orbital in the side-on structure to a filled bonding level below the Cu d$_{xy}$ orbitals in the bis-μ-oxo structure creates this new donor level. This interaction between the Cu d$_{xy}$'s and the oxo σ_u* in the bis-μ-oxo dimer is the source of the increase in Cu−O bond strength and the high covalency for this complex. The high energy of this CT indicates a large stabilization of oxo σ_u* relative to the side-on peroxo bonding scheme.[4] This O−O σ-antibonding orbital is unoccupied and located 3.743 eV (30,200 cm^{-1}) above the LUMO in the Xα calculation on the side-on peroxo structure. In contrast, it is 3.485 eV (28 100 cm^{-1}) below the same MO in the bis-μ-oxo calculation (Figure 10). This energetic stabilization is a direct result of the lengthened O···O separation in the bis-μ-oxo (2.34 Å) relative to the side-on peroxo dimer (1.41 Å). ADF 2.0.1[18] calculations indicate that as the bond length of O$_2^{2-}$ is increased from 1.41 to 2.34 Å, σ_u* is stabilized by a similar amount, 7.058 eV (57 000 cm^{-1}).

O−O Bond Cleavage Mechanism. This magnitude of the σ_u* stabilization in the bis-μ-oxo dimer drops this orbital below the d-manifold in energy to become a new donor orbital. This is similar to, but in the opposite direction, of the Mn(IV)$_2$(μ-O)$_2$ to μ-η^2:η^2 correlation drawn by Proserpio, Hoffmann, and
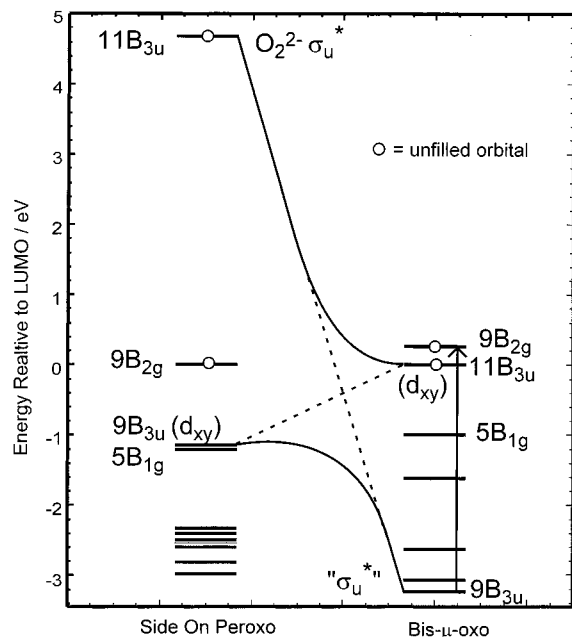
Figure 10. Orbital correlation diagram for the bis-μ-oxo/side-on peroxo isomerization. Note the net stabilization of the O_2^{2-} σ_u* orbital. Energy levels for the side-on peroxo and bis-μ-oxo dimers were scaled such that $E_{LUMO} = 0$ eV. Unfilled orbitals are indicated by (○).
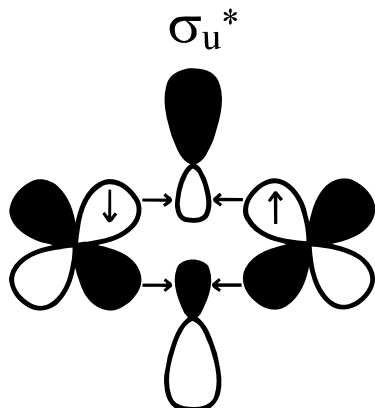
Scheme 1

Dismukes.[53] This process is an extension of the back-donation of electron density from the Cu d_{xy} orbitals into the O_2^{2-} σ_u* (Scheme 1), which was initially detected in the Cu(II)$_2$ side-on peroxo dimer and is responsible for its weak 740 cm^{-1} ν(O−O) rRaman stretch. This energetic crossover (Figure 10) results in full reductive cleavage of the peroxide to give two μ-oxo bridges and oxidation of the copper atoms to Cu(III)'s, which are stabilized by the increase in Cu/O/N covalency.

The experimental confirmation of this electronic structural model (i.e. the O_2^{2-} σ_u* crossover of the d_{xy} orbitals) for the reductive cleavage of the O−O bond comes from the determination of the geometry change ($\Delta r_{Cu-O} = +0.091$ Å and $\Delta r_{O-O} = -0.301$ Å) associated with excitation into the $\Delta E = 25\,000$ cm^{-1} CT band, the $9B_{3u}$ to $9B_{2g}$ transition (Figure 10, right). The resulting excited-state geometry is intermediate between the side-on peroxo and bis-μ-oxo structures (Figure 11), and intuitively correlates with an oxo σ_u* to Cu(III) d_{xy} LMCT assignment. This transfers electron density from the two oxo's to the two Cu(III)'s, producing an excited state which is effectively Cu$^{2.5+}$ (for a delocalized electronic description) with

(53) Proserpio, D. M.; Hoffmann, R.; Dismukes, G. C. *J. Am. Chem. Soc.* **1992**, *114*, 4374- 4382.
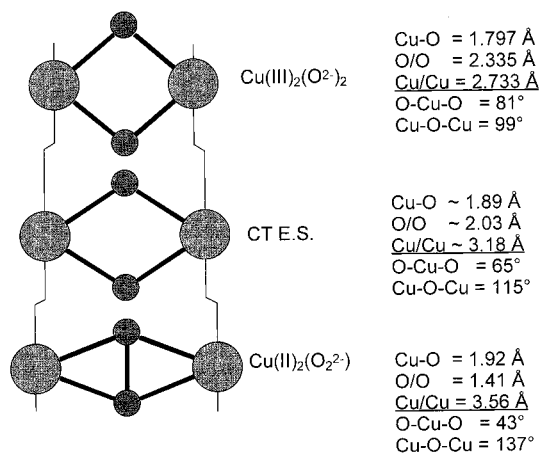
Figure 11. Correlation of the L^{MECHD} bis-μ-oxo 25 000 cm^{-1} CT excited-state geometry (center) to that of the electronic ground states of the bis-μ-oxo (top) and side-on peroxo (bottom) dimers.

corresponding oxo ligand oxidation. The large decrease of the O⋯O separation corresponds to partial O−O bond formation due to an e$^-$ being transferred out of the O−O σ-antibonding orbital.

Insight Into Interconversion. Both the side-on peroxo and bis-μ-oxo isomers can be directly observed when L^{iPr_3TACN} is used in Cu$_2$O$_2$ dimer formation.[5,6] Although calculations[10a,b] have shown these structures to be nearly isoenergetic ($\Delta E \approx 0.3$ kcal/mol), with a low barrier to interconversion (<8 kcal/mol) consistent with experiment,[5,6] this result is not universally accepted. Others calculate that the barrier to interconversion is larger (11.6 kcal/mol), with the bis-μ-oxo isomer more stable than the side-on peroxo.[10c] However, these calculations indicate a +2 charge on the Cu ions in the bis-μ-oxo dimer in contrast to experimental XAS results,[9] which demonstrate a +3 assignment. The reason the two structures have similar energies despite the large energetic stabilization of the O_2^{2-} σ_u* orbital (Figure 10) is that while O−O bonding interactions are no longer present in the bis-μ-oxo, Cu−O bonding is strengthened. The most stable configuration is determined by the energy of the Cu d_{xy} orbitals relative to the oxygen σ_u* orbital. The d_{xy} orbital energies are generally influenced by the metal coordination environment as well as the donor properties of the ligands employed. For instance, a square planar geometry will favor the low-spin d^8 Cu(III) ions of bis-μ-oxo by destabilizing the d_{xy} orbital.[3,54] Similarly, strong σ-donating ligands (i.e., amines) should favor bis-μ-oxo by simultaneously increasing the back-bonding interaction between the metals and the O_2^{2-} σ_u* orbital (the side-on peroxo HOMO, Scheme 1) and stabilizing Cu(III).

However, there exist two major geometric/electronic effects that could contribute to a large barrier to the interconversion between the side-on peroxo to bis-μ-oxo structures. As the O⋯O distance increases upon isomerization from the side-on peroxo toward the bis-μ-oxo configuration, the O_2^{2-} σ_u* orbital ($11B_{3u}$) drops in energy (Figure 10). Simultaneously, as the Cu−O and Cu−N bond lengths shorten, the Cu d_{xy} orbitals ($9B_{3u}$) are destabilized. In the bis-μ-oxo limit, these two MO's have crossed, with the oxo σ_u* deeper in energy than the d_{xy} orbitals. The symmetry-forbidden crossing of these two levels, both of B_{3u} symmetry, would be expected to result in an energetic barrier to interconversion between side-on peroxo and bis-μ-oxo.

Further, a large geometry change is expected to result from cleavage of the O−O bond upon isomerization to bis-μ-oxo.

(54) Diaddario, L. L.; Robinson, W. R.; Margerum, D. W. *Inorg. Chem.* **1983**, *22*, 1021.

The reorganization energy associated with such a geometry change is given by

$$\Delta E_i = -\tfrac{1}{2}k_i\Delta Q_i^2 \qquad (8)$$

where ΔQ_i is the dimensioned geometry change along the normal mode i, and k_i is the modal force constant. An approximation may be made to the magnitude of the reorganization energy from the LMCT excited-state distortion determined for the bis-μ-oxo dimer, which involves formation of half of the O–O bond (*vide supra*). Using the modal force constants from the normal coordinate analysis and the distortions obtained from the Heller-theory[15] fits of the rR profiles and the absorption spectrum, reorganization energies are determined along the two totally symmetric core vibrational modes: ($\Delta E_{609} = -1228$ cm^{-1}) + ($\Delta E_{118} = -1737$ cm^{-1}) = ($\Delta E_{TOT} \cong -3000$ cm^{-1}). Simply extending these results to an excited-state distortion resulting in the side-on peroxo geometry gives an approximate reorganization energy of $-10\,000$ cm^{-1} for the full ($2e^-$ reduced from peroxo) O–O bond cleavage. The magnitude of this term is also expected to contribute to a large reorganization barrier to isomerization from the side-on peroxo to the bis-μ-oxo geometry.

To rationalize the experimental observation of a low energetic barrier to interconversion, SCF Xα-SW calculations were performed on a series of geometries intermediate between the side-on peroxo and bis-μ-oxo structures. As the geometry progresses toward that of the bis-μ-oxo structure, the unoccupied O_2^{2-} σ_u^* MO is stabilized in energy relative to the Cu d-manifold. As the energetic splitting between the σ_u^* and the fully occupied $9B_{3u}$ (Cu d_{xy}) MO decreases, these orbitals mix. At a point roughly intermediate between the side-on and bis-μ-oxo geometries, these MO's are closest to one another and are equally mixed. The extent of interaction between these two levels (i.e., the energy splitting at the crossing point) indicates a large electronic coupling matrix element ($2H_{AB}$) between them. This term is calculated to be $2H_{AB} \approx 16\,000$ cm^{-1} from the splitting between the $11B_{3u}$ and $9B_{3u}$ levels at their closest point of approach (crossing point in Figure 10). The electronic coupling term is large relative to the estimated reorganization energy ($-10\,000$ cm^{-1}) predicted for full O–O bond cleavage due to significant d_{xy}/σ_u^* overlap in the bis-μ-oxo Cu$_2$O$_2$ core and will thus effectively lower the barrier to interconversion.

Electronic Structural Contributions to Reactivity. Interesting differences in reactivity are observed for the side-on peroxo and bis-μ-oxo dimers. The side-on peroxo dimer is thought to be kinetically more reactive toward the electrophilic hydroxylation of substrates,[12] while the bis-μ-oxo dimer is more reactive with respect to H-atom abstraction (HA).[6] The electrophilic reactivity has been addressed using frontier molecular orbital (FMO) theory,[12] which indicates an increase in charge donation from the coppers to the oxygens in the bis-μ-oxo core, reducing (but not precluding) the effectiveness of electrophilic attack by this species. Electrophilic reactivity has, however, recently been reported for a bis-μ-oxo dimer.[55] This current study provides insight into the electronic structural contributions to the relative HA reactivity of the two isomers.

Two factors should contribute to the rate of H-atom abstraction by a metal complex: the thermodynamic driving force for the reaction, and the Franck–Condon (FC) barrier. Both side-on peroxo and bis-μ-oxo structures can be anticipated to give the same product as a result of HA, a Cu(II,III)(μ-O)(μ-OH)
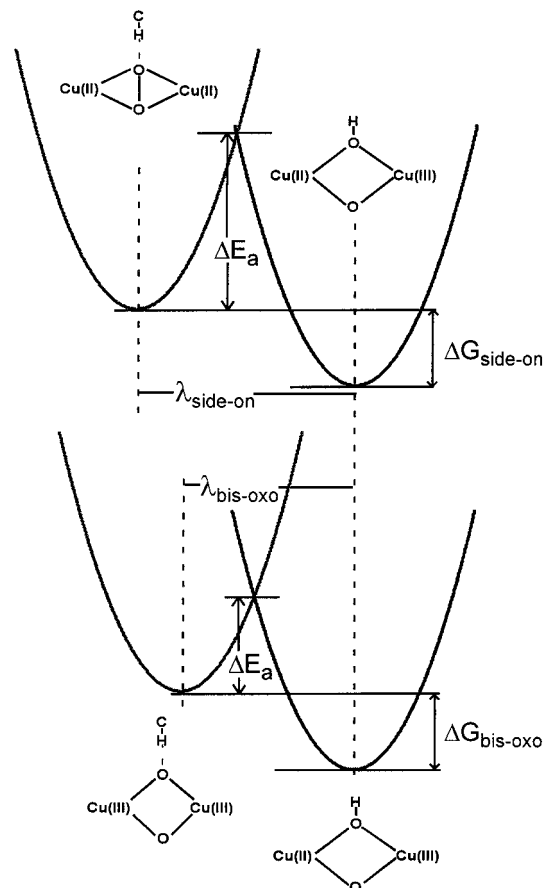
Figure 12. Qualitative potential energy surfaces for the H-atom abstraction reaction of the side-on peroxo (top) and bis-μ-oxo (bottom) dimers, showing the effects of geometric distortion (λ_i) and thermodynamic driving force (ΔG_i) upon the activation energy (ΔE_a). For $\lambda_{bis-oxo} < \lambda_{side-on}$ and assuming $\Delta G_{bis-oxo} \cong \Delta G_{side-on}$, ΔE_a(bis-oxo) < ΔE_a(side-on).

core (Figure 12).[14] One possible formulation of the driving force for this proton-coupled electron transfer is in terms of the pK_A of the product and the reduction potential of the abstracting metal complex.[56,57] It has proven difficult to measure the reduction potentials for the side-on peroxo and bis-μ-oxo isomers. A wide difference in irreversible potentials has been observed.[8,58] Different ligand environments preferentially stabilize one isomer over the other. For at least one ligand system (L^{iPr_3TACN}), the isomeric side-on peroxo and bis-μ-oxo species exist in a rapid equilibrium at near-equivalent concentrations,[5,6] indicating similar free energies. Thus, the potentials for the 1 e^- reductions of side-on peroxo and bis-μ-oxo to the same species should be similar. Assuming a similar 1 e^-/1 H$^+$ reduced product, the net difference in driving force for HA from a substrate by the side-on peroxo and bis-μ-oxo species will be small.

The second contribution to the HA reactivity of the side-on peroxo and bis-μ-oxo isomers, dominant in the absence of a large difference in the thermodynamic driving force, is the FC barrier to the electron-transfer reaction. A larger geometry change is associated with the reaction coordinate of the side-on peroxo relative to bis-μ-oxo, as formation of the final product

(55) Holland, P. L.; Rodgers, K. R.; Tolman, W. B. *Angew. Chem., Int. Ed.* **1999**, *38*, 1139- 1142.

(56) Bordwell, F. G.; Zhang, X.-M.; Satish, A. V.; Cheng, J.-P. *J. Am. Chem. Soc.* **1994**, *116*, 6605−6610.

(57) Gardner, K. A.; Mayer, J. M. *Science* **1995**, *269*, 1849−1851.

(58) Karlin, K. D.; Tyeklár, Z.; Farooq, A.; Haka, M. S.; Ghosh, P.; Cruse, R. W.; Hayes, J. C.; Toscano, P. J.; Zubieta, J. *Inorg. Chem.* **1992**, *31*, 1436−1451.

complex necessitates cleavage of the O–O bond in the former isomer. It was previously suggested[14] that the FC barrier corresponding to this cleavage, unnecessary in the bis-μ-oxo core, contributes to the diminished HA reactivity of the side-on peroxo dimer. From the reorganization energy of the bis-μ-oxo 25 000 cm^{-1} CT excited-state distortion we estimate that there is a significant FC barrier associated with the addition of 1 e$^-$ to the side-on peroxo dimer. A large electronic coupling element (H_{AB}) between the 9B_{3u} (d_{xy}–d_{xy}) and 11B_{3u} (σ_u^*) levels (Figure 10) decreases the barrier to interconversion between the side-on peroxo and bis-μ-oxo species which would otherwise have resulted form this large reorganization energy (*vide supra*). However, addition of 1 e$^-$ to the side-on peroxo complex involves the 9B_{2g} (d_{xy}+d_{xy}) as the redox-active level (Figure 10, left), which by symmetry cannot electronically couple to the 11B_{3u} orbital. Thus, geometric relaxation to the product shown at the right of Figure 12 involves cleavage of the O–O bond and transfer of the e$^-$ between the 9B_{2g} and 11B_{3u} orbitals, which should result in a large FC barrier. In the bis-μ-oxo structure the O–O bond is already cleaved and the redox-active orbital is 11B_{3u}, leading to a smaller barrier to HA by this isomer (Figure 12, bottom). Under conditions of similar thermodynamic driving forces, the smaller FC barrier to reaction for the bis-μ-oxo will result in a greater HA reactivity relative to the side-on peroxo dimers, as observed experimentally.[6] H-atom abstraction is, however, still possible for a side-on structure, but with a larger barrier.

Summary

Cu$_2$ bis-μ-oxo dimer formation is driven by back-bonding into the O$_2^{2-}$ σ_u^* orbital, which is favored by high Cu d$_{xy}$ energies resulting from strong σ-donor ligands and/or square planar geometry. Consistent with XAS results, the spectroscopic and computational description is of a Cu(III)$_2$ dimer strongly stabilized by a new donor interaction relative to the Cu(II)$_2$ side-on peroxo-bridged, μ-η^2:η^2 dimer. A new, intense charge-transfer transition observed at 25 000 cm^{-1} for the [(L^{MECHD}-Cu^{III})$_2$(μ-O)$_2$]$^{2+}$ complex corresponds to this additional donor interaction which reflects the higher bis-μ-oxo metal–ligand covalency and is assigned as the oxo σ_u^* (fully populated in the bis-μ-oxo dimer) to Cu(III) d$_{xy}$ CT transition. Significantly, from an analysis of the excited-state geometry of the σ_u^* to d$_{xy}$ CT transition, this excitation leads to partial formation of the O–O bond. This experiment demonstrates that the reversible formation of the O–O bond involves changes in the e$^-$ population of the O$_2^{2-}$ σ_u^* orbital. The different electronic structures of the side-on peroxo and bis-μ-oxo dimers contribute to the observed differences in reactivity for the two isomers, where the latter has a lower reorganizational energy barrier to H-atom abstraction.

Supporting Information Available: Cartesian input coordinates of the [(NH$_3$)$_4$Cu$_2$(μ-O)$_2$]$^{2+}$ model used in the SCF Xα-SW calculations, the ^{16}O$_2$/^{18}O$_2$ Raman spectra of the high-frequency overtone and combination bands of the L^{MECHD} dimer, and the resonance Raman spectra showing the relative enhancement behavior of the ν_1 (= 133 cm^{-1}) peak of the L^{TMPD} dimer and its overtone, 2ν_1 (= 266 cm^{-1}) (PDF). This material is available free of charge via the Internet at http://pubs.acs.org.

JA9918425